ISTANBUL TECHNICAL UNIVERSITY ★ GRADUATE SCHOOL

INTRA-PATIENT AND INTER-PATIENT ADAPTIVE CONTROL OF HYPNOTIC STATES DURING TOTAL INTRAVENOUS ANESTHESIA

M.Sc. THESIS

Bora AYVAZ

Department of Control and Automation Engineering

Control and Automation Engineering Programme

JUNE 2024

ISTANBUL TECHNICAL UNIVERSITY ★ GRADUATE SCHOOL

INTRA-PATIENT AND INTER-PATIENT ADAPTIVE CONTROL OF HYPNOTIC STATES DURING TOTAL INTRAVENOUS ANESTHESIA

M.Sc. THESIS

Bora AYVAZ
(504221105)

Department of Control and Automation Engineering

Control and Automation Engineering Programme

Thesis Advisor: Assoc. Prof. Dr. Ali Fuat Ergenç

JUNE 2024

İSTANBUL TEKNİK ÜNİVERSİTESİ ★ LİSANSÜSTÜ EĞİTİM ENSTİTÜSÜ

TOTAL İNTRAVENÖZ ANESTEZİ SIRASINDA HİPNOTİK DURUMLARIN HASTA İÇİ VE HASTALAR ARASI UYARLAMALI KONTROLÜ

YÜKSEK LİSANS TEZİ

Bora AYVAZ
(504221105)

Kontrol ve Otomasyon Mühendisliği Anabilim Dalı

Kontrol ve Otomasyon Mühendisliği Programı

Tez Danışmanı: Doç. Dr. Ali Fuat Ergenç

HAZİRAN 2024

Bora AYVAZ, a M.Sc. student of ITU Graduate School student ID 504221105 successfully defended the thesis entitled "INTRA-PATIENT AND INTER-PATIENT ADAPTIVE CONTROL OF HYPNOTIC STATES DURING TOTAL INTRAVENOUS ANESTHESIA", which he/she prepared after fulfilling the requirements specified in the associated legislations, before the jury whose signatures are below.

Thesis Advisor :	**Assoc. Prof. Dr. Ali Fuat Ergenç** Istanbul Technical University	.....
Jury Members :	**Prof. Dr. Mustafa Doğan** Istanbul Technical University	.....
	Asst. Prof. Dr. Kerem Altun Yıldız Technical University	.....
		.....

Date of Submission : **16 May 2024**
Date of Defense : **11 June 2024**

To my family and Beyza,

FOREWORD

I am grateful to my advisor, Assoc. Prof. Dr. Ali Fuat ERGENÇ, who has guided me to improve myself as a human and an engineer for nearly six years since the first year of my bachelor's degree. He has become my mentor, and the years we spent in the laboratory have taught me everything I know about being an engineer. I appreciate Asst. Prof. Dr. Erhan YUMUK for his support in helping me select my thesis topic and for his guidance throughout the research and writing process. I also appreciate the jury members of my dissertation, Prof. Dr. Mustafa DOĞAN and Asst. Prof. Kerem ALTUN for their valuable comments.

The people who supported me throughout my education, guided me in choosing my career path, and shaped me into the person I am today are my beloved father, M.D. Levent AYVAZ and my brother Arda AYVAZ. I thank them and my whole family for supporting me for my whole life and being there whenever I need. I also specially thank Beyza YAPAKÇI for making my hard and stressful times easy and beautiful. Finally, I am thankful to my friends and colleagues, Res. Asst. Ramazan Kaya and Res. Asst. Ayşe Duman Mammadov for their limitless support.

JUNE 2024

Bora AYVAZ
(Research Assistant)

TABLE OF CONTENTS

ABBREVIATIONS

TIVA : Total Intravenous Anesthesia
MPC : Model Predictive Control
PID : Proportional Integral Derivative
TIVA : Total Intravenous Anesthesia
CL-TIVA : Closed Loop Total Intravenous Anesthesia
PID-TIVA : CL-TIVA with PID Controller
ADP-TIVA : CL-TIVA with Adaptive Controller
MRAC-TIVA: CL-TIVA with Model Reference Adaptive Control
MPC-TIVA : CL-TIVA with Model Predictive Controller
SFC-TIVA : State Feedback Control of Total Intravenous Anesthesia
ODE : Ordinary Differential Equation
PK : Pharmacokinetic
PD : Pharmacodynamic
EEG : Electroencephalography
BIS : Bispectral Index
lbm : Lean Body Mass
CE : Effect-side concentration
LSE : Least squares error
ARX : Autoregressive model with exogenous input
LTI : Linear time invariant
LTI-RTDS : linear time-invariant retarded time delay system
DARX : Delayed autoregressive model with exogenous input
mg : milligrams
IAE : Integral-Absolute-Error
CE : Effect-side concentration
GM : Gain margin
PM : Phase margin
DB : Database
MRAS : Model reference adaptive system
MRAC : Model reference adaptive controller
L-MRAS : Lyapunov's Based MRAS
L-MRAC : Lyapunov's Based MRAC
C-Time : Continious-time
CCF : Controllable Canonical Form
PK : Pharmacokinetical
PD : Pharmacodynamical

SYMBOLS

A,**B**,**C**,**D**	: Linear system matrices
q	: Quantity of solute
A_q	: Membrane surface area
D_q	: Diffusion coefficient
dx_q	: Membrane thickness
K_q	: Flow transfer rate parameter
k_{ij},C_{li}	: Schinder drug transfer rate parameters
V_1,V_2,V_3	: Compartment volumes
E_0,E_{max},C_{50},γ	: Hill-curve coefficients
k_h,d_h	: First order shifted linear function parameters
K_p,K_d,K_i,K_b	: PID controller parameters
K_f,M	: State feedback controller gains
α,β	: Free design parameters for MRAC
τ	: Continuous time delay
d	: Discrete time delay
λ	: Eigenvalue
s_i	: Pole
t	: Time
r	: Reference
e	: Error
V	: Lyapunov function
s	: Complex frequency parameter in Laplace transform

LIST OF TABLES

LIST OF FIGURES

Page

INTRA-PATIENT AND INTER-PATIENT ADAPTIVE CONTROL OF HYPNOTIC STATES DURING TOTAL INTRAVENOUS ANESTHESIA

SUMMARY

Total intravenous anesthesia refers to administering medications to induce a state of controlled unconsciousness or analgesia during surgical or medical procedures. These medications target the nervous system, producing various effects such as pain relief, amnesia, and muscle relaxation. General anesthesia renders the patient completely unconscious and unaware of their surroundings.

The input to the total intravenous anesthesia system is the rate of Propofol, and the output is the bispectral index when considered as a control system. The patient's hypnotic state can be controlled by taking the BIS as feedback. During surgery, stimuli such as scalpel cuts affect the system as output disturbances, while blood loss affects the system as parameter uncertainty and time-variant parameters.

The total intravenous anesthesia system can be considered one of the most complex control systems due to its time-varying characteristics, intra-patient and inter-patient variability, unpredictability, and model uncertainty.

Controlling the patient's hypnotic state in anesthesia faces many challenges, including patient-dependent variables, uncertain time delays, drug-dependent dynamics, and stability issues. Despite the development of various control systems such as PID control, MPC, and various adaptive control methods, the inability to ensure intra-patient and inter-patient validity remains one of the biggest obstacles to applying anesthesia systems with automatic control features to broader patient groups. Therefore, new adaptive control structures with minimal patient parameter dependency are needed.

In this thesis, two primary objectives can be mentioned for the modeling and control of the total intravenous anesthesia system. The first is to propose a model improvement method that enhances the correlation with real surgical results by adding output delays to the mathematical patient models of total intravenous anesthesia based on real surgical patient data. The second is to propose a model reference adaptive control structure for the inter-patient adaptive control of closed-loop total intravenous anesthesia systems and to prove that the proposed structure can achieve more robust results in anesthesia control compared to traditional PID controllers.

The proposed methodology for determining the delay time of delayed patient models involves estimating patient model parameters obtained as parametric transfer functions using the least squares method from the VitalDB database containing real surgical data. The delay value that produces the highest correlation with real surgical data is accepted as the individual delay value of each patient. The validity of delayed models is proven

by comparing the correlations between the outputs of delayed and non-delayed models and real surgical output data.

The model reference adaptive control system structure has been integrated into closed-loop total intravenous anesthesia to ensure intra-patient and inter-patient control validity. The model reference adaptive control structure for total intravenous anesthesia is based on an observer-based state feedback controller. The adaptation laws created using Lyapunov's stability theory adjust the state feedback controller gains to ensure inter-patient validity. The model reference adaptive controller has been applied to total intravenous anesthesia and tested on a database of 24 patients and patients identified by VitalDB under conditions of stimulus disturbances and blood loss.

Correlation analysis results show that patient models with output delays in pharmacokinetic-pharmacodynamic analysis, with the bispectral index as the output, exhibit stronger correlations with real patient data from VitalDB. The importance of this result increases, especially considering that the bispectral index is the only measurable output value. In addition, the model reference adaptive control system proposed in this thesis has improved the control of total intravenous anesthesia, producing more robust and desirable results compared to the common PID controllers. The model reference adaptive control system for total intravenous anesthesia suggested in this thesis can be used to develop and manage the patient's hypnotic state during total intravenous anesthesia.

TOTAL İNTRAVENÖZ ANESTEZİ SIRASINDA HİPNOTİK DURUMLARIN HASTA İÇİ VE HASTALAR ARASI UYARLAMALI KONTROLÜ

ÖZET

Total intravenöz anestezi, cerrahi veya tıbbi işlemler sırasında kontrollü bilinçsizlik veya analjezi durumunu indüklemek için ilaçların uygulanmasını ifade eder. Bu ilaçlar sinir sistemini hedef alarak ağrı giderme, amnezi ve kas gevşemesi gibi çeşitli etkiler üretir. Genel anestezi, hastayı tamamen bilinçsiz ve çevresinden habersiz hale getirir.

Genel anestezi, tüm süreç intravenöz anestezi ile başlatılıp bitirilirse, total intravenöz anestezi (TIVA) olarak adlandırılır. Cerrahi sırasında modern genel anestezinin üç ana durumu tanımlanabilir: hipnoz, analjezi ve arefleksi. Hipnoz, bilinç kaybını içerir ve prosedür sırasında farkındalığı ve hafıza oluşumunu önler, burada ana ajan Propofol'dür. Bilinçsizlik derinliği, Elektroensefalografi (EEG) sinyallerinin bispektral analiziyle elde edilen Bispektral indeks (BIS) ile ölçülür. Analjezi, ağrı hissetmeme durumudur ve ağrı yollarını keserek hastanın ağrı hissetmesini önler.

TIVA, dört aşamadan oluşur: premedikasyon, indüksiyon, idame ve uyanma. Premedikasyon, hastanın prosedüre hazırlandığı aşamadır ve uyanma, hastanın anesteziden kurtulduğu aşamadır; bu aşamalarda ilaç enjeksiyonu aktif değildir. İndüksiyon aşamasında, hastayı bilinçten cerrahi için yeterli bilinçsizlik seviyesine geçirmek için yoğun hipnotik ve analjezik ilaçlar kullanılır. Bunu takiben, idame aşamasında, hem bilinçsizlik hem de ağrı baskılanması ile karakterize edilen yeterli cerrahi anestezi durumunu sürdürmek için sürekli ilaç uygulaması yapılır. Son olarak, ilaç uygulamasının durdurulmasıyla hastanın yavaş yavaş bilincine döndüğü uyanma aşaması gerçekleşir.

İdeal bir anestezik ilaç anesteziyi hızla indükleyip sonlandırmalı, hızlı bir şekilde uyanma ve temel fonksiyonlara dönüş sağlamalıdır. Propofol, vücuttan hızla metabolize edilip atıldığı için hipnozun ana ajanı olarak kabul edilir. Anestezi sırasında gerekli bilinçsizlik seviyesine ulaşmak ve bunu korumak için hipnoz durumunu izlemek ve takip edebilmek. İdeal bir anestezi monitörü hipnoz derinliğini doğru bir şekilde takip etmelidir. Bu durumları izlemek için ana yöntem, anesteziklerin merkezi sinir sistemi üzerindeki farmakodinamik etkilerini ölçmek amacıyla elektroensefalogram (EEG) sinyallerinin istatistiksel analiziyle elde edilen sayısal bir değer olan bispektral indekstir (BIS).

Total intravenöz Anestezi bir kontrol sistemi olarak ele alındığında sistemin girişi Propofol oranı, sistemin çıkışı ise bispectral indeks olamaktadır. Bispektral indeks kontrol edilebildiğinde hastanın hipnotik durumu da kontrol edilmiş olur. Ameliyat esnasında bıçak kesiği gbii uyaranlar sistemi çıkış bozucusu olarak etkilerken, kan kaybı sistemi parametre belirsizliği ve zamana bağlı parametre değişimi olarak etkiler.

Total intravenöz anestezi sistemi, zamanla değişen özelliklere, hasta içi ve hastalar arası farklılıklara, öngörülemezliğe ve model belirsizliğine sahip olmasıyle, kontrol sistemleri arasında en karmaşık olanlardan biri olarak kabul edilebilir.

Anestezi süreçlerini kontrol etmek ve otomatikleştirmek için hastalardaki ilaç dağılımının dinamiklerini temsil eden matematiksel modeller ve diferansiyel denklemler elde edilmelidir. İlacın vücudun farklı dokularına yayılması, komşu dokular arasında farklı yayılma hızları kullanılarak kompartımanlar kullanılarak modellenebilir. Bu nedenle, kompartıman modellemesi, insan dolaşım sistemindeki ilaç dağılım dinamiklerini modellemek için doğrusal farmakokinetik modeller üreten faydalı bir yöntemdir.

Anestezi için kompartıman modelleri, çoğunlukla farmakokinetik ve farmakodinamik bloklardan oluşur. farmakokinetik, ilaç konsantrasyonlarını intravasküler kan ve yağ-kas alt biyolojik sistemlerinde tanımlarken, farmakodinamik, kan sistemindeki ilaç konsantrasyonunun hasta üzerindeki etkilerini tanımlar. farmakokinetik ve farmakodinamik modelleri, doğrusal bir model ve statik bir doğrusal olmayan filterinin birleşimi olarak birbirine eklenerek anestezik modeli tamamlar. Anestezik modelin doğrusal kısmının çıktısı, etki-bölgesi ilaç konsantrasyonudur. Farmakodinamik modelin doğrusal olmayan kısmı, etki-bölgesi konsantrasyonlarını giriş olarak alan ve Hill eğrisi kullanarak BIS çıktısı üreten bir filtre olarak modele entegre edilebilir.

Ameliyatlar sırasında vücut sıvısında, çoğunlukla kan kaybından kaynaklanan bir değişiklikten bahsetmek mümkündür. Bu nedenle, cerrahi sırasında kanama nedeniyle kan hacmi zamanla değiştiği için anestezik model zamanla değişen bir sistem olarak kabul edilebilir. Cerrahi sırasında kan kaybına ek olarak uyandırıcı uyaranlar şeklinde bozucular meydana gelir ve bu uyaraların anestezi sürecinin idame aşamasında meydana geldiği kabul edilir. Bu tür bozucuların ve kan kaybının etkisinin kapalı çevrim anestezi sürecinde kontrolör tarafından giderilmesi beklenir.

Anestezide hastanın hipnotik durumunun kontrol edilmesi, hastaya bağlı değişkenler, belirsiz zaman gecikmeleri, ilaca bağlı dinamikler ve stabilite gibi birçok zorluk ile karşı karşıyadır. PID kontrol, MPC ve çeşitli uyarlamalı kontrol yöntemleri gibi geliştirilen çeşitli kontrol sistemlerine rağmen, hasta içi ve hastalar arası geçerlilik sağlama yetersizliği, anestezi sistemlerinin otomatik kontrol özellikleriyle daha geniş hasta gruplarına uygulanmasının önündeki en büyük engellerden biridir. Bu nedenle, hasta parametre bağımlılığı en az olan yeni uyarlamalı kontrol yapıları gerekmektedir.

Bu tez kapsamında total intravenöz anestezi sisteminin modellenmesi ve kontrolü için temel olarak 2 hedeften bahsedilebilir. Bunlardan ilki, total intravenöz anestezi matematiksel hasta modellerine çıkış gecikmelerinin eklenmesiyle gerçek cerrahi hasta verileri üzerinden, gerçek sonuçlara olan korelasyonu arttırabilen bir model iyileştirmesi metodu ortaya koymaktır. İkincisi ise kapalı çevrim total intravenöz anestezi sistemlerinin hastalar arası uyarlamalı kontrolü için bir model referans adaptif kontrol yapısı önerilmesi ve önerilen yapının anestezi kontrolünde geleneksel PID kontrolörlerden daha dayanıklı sonuçlar elde edebildiğinin kanıtlanmasıdır.

Hastaların doğrusal modellerini tanımlamak ve doğrusal olmayan Hill eğrisinin doğrusal bir yaklaşımını en küçük kareler hata yöntemiyle bulmak mümkündür. Bir ARX model yapısı, doğrusal model ile regressor ve parametre vektörlerini elde etmek

amacıyla veritabanındaki verilerden propofol oranı girişi ve etki tarafı konsantrasyonu arasındaki doğrusal modeli tanımlamak için oluşturulmuştur. Doğrusal olmayan Hill eğrisi, CE ve BIS cerrahi hasta verileri kullanılarak birinci dereceden kaydırılmış doğrusal bir fonksiyon olarak yaklaşılabilir.

Korelasyon analizi, sonuçlar arasındaki ilişkiyi analiz etmek için yararlı bir yöntemdir. Bu nedenle, sonuçların korelasyonunu ve tanımlanan modellerin geçerliliğini göstermek amacıyla, VitalDB'den alınan gerçek çıkış verileri ile tanımlanan model çıktıları arasındaki korelasyon analizi yapılmıştır. Korelasyon analizi sonuçları göstermiştir ki CE çıkışı için yapılan en küçük kareler yöntemi sonucunda elde edilen modeller, gerçek cerrahi veriler ile güçlü veya çok güçlü korelasyon katsayıları üretmiştir. Ancak BIS çıkışı için yapılan en küçük kareler yöntemi sonucunda elde edilen modellerin tamame gerçek veriler ile istenen korelasyona sahip olamamıştır. Bu duruma BIS monitörü üzerinden alınan ölçüm gürültüleri ve monitör gecikmelerinin sebep olmuş olabileceği düşünülmüştür. Buna göre, BIS çıkışlı doğrusallaştırılmış hasta modeline monitör gecikmesi eklenmesi sayesinde, model çıkışları ile gerçek veriler arasında daha yüksek korelasyon elde edilebileceği hipotezi üretilmiştir.

Gecikmeli hasta modellerinin gecikme süresinin belirlenmesi için önerilen metodoloji, parametrik transfer fonksiyonu olarak elde edilen hasta modeli parametrelerinin en küçük kareler yöntemi ile gerçek cerrahi veriler içeren VitalDB veritabanından kestirilmesini içerir. Gerçek cerrahi verilerle en yüksek korelasyonu üreten gecikme değeri, her hastanın bireysel gecikme değeri olarak kabul edilir. Gecikmeli modellerin geçerliliği, gecikmeli ve gecikmesiz model çıktıları ile gerçek cerrahi çıktı verileri arasındaki korelasyonları karşılaştırarak kanıtlanır. Korelasyon analizi sonuçları, farmakokinetik-farmakodinamik hasta modellerinde çıkış gecikmelerini içeren bispektral indeks çıkışlı hasta modellerinin, VitalDB'den alınan gerçek hasta verileriyle daha güçlü korelasyonlar gösterdiğini göstermektedir. Özellikle bispektral indeks değerinin ölçülebilen tek çıkış değeri olduğu düşünüldüğünde bu sonucun önemi artmaktadır.

Model referans adaptif kontrol sistemi yapısı, hasta içi ve hastalar arası kontrol geçerliliği sağlamak amacıyla kapalı çevrim total intravenöz anesteziye entegre edilmiştir. Total intravenöz anestezi için model referans adaptif kontrol yapısı, gözlemci tabanlı bir durum geri besleme kontrolörüne dayanmaktadır. Lyapunov'un kararlılık teorisi kullanılarak oluşturulan uyarlama yasaları, hastalar arası geçerliliği sağlamak için durum geribesleme kontrolörünün kazançlarını ayarlamaktadır. Model referens adaptif kontrolör, Total intravenöz anesteziye uygulanmış ve uyaran bozucuları ile sürekli kan kaybı durumlarında, 24 hastalık bir veri tabanı ve VitalDB tarafından tanımlanan hastalar üzerinde test edilmiştir.

Bunun yanında tez kapsamında önerilen model referans adaptif kontrol sistemi, total intravenöz anestezi kontrolünü iyileştirerek yaygın PID-TIVA kontrolörüne kıyasla daha dayanıklı ve istenilen sonuçlar üretmiştir. Total intravenöz anestezi için model referans adaptif kontrol sistemi, total intravenöz anestezi sırasında hastanın hipnotik durumunu geliştirmek ve yönetmek için kullanılabilir.

1. INTRODUCTION

Anesthesia refers to administering medications to induce a state of controlled unconsciousness or analgesia during surgical or medical procedures. These medications target the nervous system, producing various effects including pain relief, amnesia, and muscle relaxation. General anesthesia renders the patient completely unconscious and unaware of their surroundings, while regional anesthesia numbs a specific area of the body.

Modern anesthesia began with the use of ether and chloroform gases. The successful use of these gases in endotracheal incubation ensured airway and patient safety. Parallel to gas inhalation using anesthesia delivery systems such as Norton Masks, the development of supporting anesthetic drugs delivered intravenously continued. The first intravenous anesthesia was conducted with choral hydrate, and the combination of morphine-scopolamine was common during the Great War. However, such drugs have serious side effects, especially on the cardiovascular system. The usage of Propofol (2,6-diisopropophenol, $C_{12}H_{18}0$) began in 1977 and showed significant improvement in shortening recovery periods and suppressing side effects [1].

It is possible to show three main states of modern general anesthesia during surgery: hypnosis, analgesia, and areflexia. Hypnosis is the loss of consciousness and the hypnotic state prevents awareness and memorization during the surgery. The main agent of hypnosis is Propofol. The depth of unconsciousness is represented by the Bispectral index (BIS), which can obtained by bispectral analysis of Electroencephalography (EEG) signals. Analgesia refers to the inability to feel pain. The primary function of analgesia is to interrupt pain pathways, thereby preventing the patient from experiencing pain [2]. The absence of pain can be indexed with Ramsay Agitation Score (RASS), and the main agent of analgesia is Remifentanil. Areflexia is the loss of reflexes accomplished by the neuromuscular blockade. Areflexia prevents the occurrence of involuntary muscle contraction by reflexes. The neuromuscular

blockade can be achieved with curare and atracurium. The main focus of this study is on the hypnotic state, where the administrated input is Propofol and the output is the BIS.

The ideal anesthetic agent embodies several crucial characteristics for optimal efficacy and safety. It should rapidly induce and cease anesthesia, allowing for rapid emergence and prompt return to baseline function. Additionally, it should offer analgesia even at lower concentrations, possess antiemetic properties to prevent nausea and vomiting, and cause minimal depression of the cardiovascular and respiratory systems. Furthermore, it should lack active metabolites, undergo metabolism independent of specific organs, and be easily titratable for precise dosing. Compatibility with neuromuscular blocking drugs, absence of toxicity to other organs, and anti-inflammatory and antioxidant effects are paramount. A long shelf life and no hypersensitivity reactions or histamine release add to its desirability and safety profile [3].

Human studies showed that Propofol is metabolized and eliminated rapidly from the body [4]. The experiments conducted using a radioactive sub-anesthetic dose of Propofol show that the Propofol is metabolized as %84 under 30 minutes [5], which can be considered rapid. Moreover, the elimination of Propofol from the human body happens nearly 10 times faster than Sodium thiopental, another general anesthetic drug [6]. Administration of propofol usually starts with a bolus injection and continues either inhalant or intravenous anesthesia. It witnessed a decrease in blood pressure and loss of eyelid reflex after bolus injection [4]. General anesthesia is called total intravenous anesthesia (TIVA) if the process starts and finishes with intravenous anesthesia, mostly with Propofol and Remifentanil.

It is possible to mention 4 phases during TIVA. These phases can be classified as pre-medication, induction, maintenance, and emergence [2]. Pre-medication is when the patient gets ready for the procedure, and emergence is when the patient recovers from anesthesia. Therefore, the drug injection is not active during the pre-medication and emergence phases. The induction phase of anesthesia utilizes the administration of concentrated hypnotic and analgesic medications to patients from

a state of consciousness to one sufficient unconsciousness for the intended surgical procedure [7]. Following induction, the maintenance phase employs continuous administration of medications to sustain a state of adequate surgical anesthesia characterized by both unconsciousness and pain suppression. This phase is then followed by emergence, where the cessation of drug delivery allows for the patient's gradual return to consciousness [7]. The anesthetic agents can be administered to the patient's body using manual or automated syringe pumps during the induction and maintenance phases. The automated syringe pumps can inject the desired amount of drug with their closed-loop drug-rate control systems. At present, the administration of drugs through computers is achieved using open-loop target-controlled infusion (TCI) systems. This represents the initial phase towards the automation of drug delivery [8].

Experiments with an average age of $71(62-82)$, male dominant (22M, 3F) elderly propofol-propofol general anesthesia group show that the induction phase takes 4.6 minutes with a standard deviation ± 1.7. The dose of $2.2 \pm 0.5(mg/kg)$ bolus propofol was injected into this patient group in the induction phase, and the total anesthesia took 40 ± 20 minutes, depending on the surgical procedure. In this patient group, the emergence phase took 6.8 ± 2.9 minutes [9].

It is important to monitor and track the state of hypnosis to reach and maintain a required state of unconsciousness during anesthesia. Maintaining optimal anesthetic depth is paramount, and insufficient anesthesia can lead to a distressing experience of awareness and pain during surgery. At the same time, excessive administration can compromise blood flow to vital organs. Given the inherent risks associated with anesthetic medications, close monitoring of the anesthetic state is essential [10]. The ideal anesthesia monitor should reliably anticipate awareness onset, accurately track anesthetic levels and hypnosis depth, exhibit 100% sensitivity and specificity, work universally across anesthetics, resist interference from non-anesthetic drugs, cater to diverse patients, maintain stability, reject artifacts automatically, offer real-time response, require no frequent calibration, and present results in an easily understandable format [10], [11].

A direct method to measure the hypnotic state is not possible. Ensuring adequate hypnosis may necessitate the use of cortical suppression monitors. These tools track the evolving effects of anesthetic agents on the brain, allowing for targeted adjustments to maintain the desired level of unconsciousness [12]. EEG, which measures electrical activity in the brain, offers a potential window into the hypnotic state. This is because changes in cortical activity, believed to mirror a patient's level of hypnosis, can be observed through EEG recordings. The EEG can reveal alterations in how the brain processes sensory information during hypnosis [13].

The methods using EEG signals to measure the depth of anesthesia have developed using power spectrum analysis such as the median edge frequency [14,15] and the spectral edge frequency [16], [13]. Despite the variety of methods, bispectral analysis (BIS) is one of the most common one. The Bispectral Index (BIS) is a numerical value derived through statistical analysis intended to gauge the pharmacodynamic impact of anesthetics on the central nervous system.

The BIS value changes between 100 and 0, where 100 relates to full awakeness, and 0 relates to full hypnosis. According to the recorded data, none of the patients were found to be conscious when their BIS value was below 65. Conversely, there were no observations of unconsciousness when the BIS value was higher than 70 [17]. Maintaining the BIS within the range of 40-60 is generally recommended during anesthesia for a wide range of surgical procedures [12,18]. The BIS value intervals are explained in Table 1.1 [19].

Table 1.1 : BIS value intervals and Hypnotic States [19]

BIS Range	Hypnotic State
$70-100$	Awake Light to Moderate Sedation
$60-70$	Light Hypnotic State Low Probability of Recall
$40-60$	Moderate Hypnotic State Unconscious
$0-40$	Deep Hypnotic State

Ranging from 0 to 100, higher values (70-100) signify wakefulness or the resting state, applicable during awake procedures or emergence from general anesthesia. In the

range of 60-70, patients experience a light hypnotic state with a low likelihood of recall, suitable for light anesthesia. As the BIS drops to 40-60, individuals enter a moderate hypnotic state, rendering them unconscious, ideal for maintaining anesthesia during surgical procedures. A BIS below 40 indicates a deep hypnotic state necessary for profound anesthesia and achieving burst suppression, which is crucial in certain neurosurgical or critical care scenarios.

Propofol concentrations in blood plasma can be estimated using BIS values. Other methods, such as electrochemical and optical, can also be used to measure propofol concentrations directly in blood plasma. One of the commonly used techniques to detect and measure the levels of propofol in plasma is high-performance liquid chromatography (HPLC) [20]. HPLC can be combined with fluorometric detection [21], UV photometry [22], and electrochemical measurement using a mixture of methanol and an acidic buffer [23]. The propofol's itself and the amount of propofol have detected using Gibbs reaction-based spectrophotometric detection [24]. Moreover, the propofol expired in the air with the patient's exhalation during TIVA can be measured using ion-molecule reaction mass spectrometry [25]. The use of electrochemical methods offers greater sensitivity but presents considerable obstacles in comparison to BIS. [20].

This section has introduced the development of modern anesthesia, the main states of anesthesia, ideal anesthetic agents, propofol usage, TIVA, the phases of TIVA, anesthesia monitors, BIS, and other measurement methods of plasma concentrations so far. The TIVA for regulating anesthesia states can be summarized using an input-output block diagram from a control engineer's perspective as seen in Figure 1.1 [26]. The surgical stimulus and blood losses during surgeries can be considered disturbances in this diagram.

The patient's hypnotic state can be controlled when the input is considered to be Propofol and the output is BIS. The stimulus affects the system as an output disturbance, and blood loss affects the system as a parametric uncertainty and time-variant. Controlling the hypnotic state of anesthesia offers valuable study

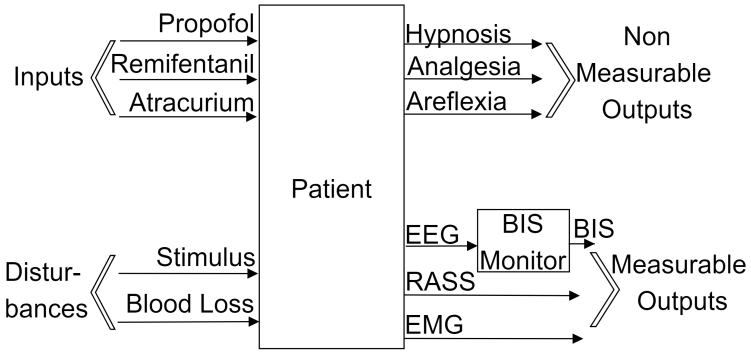

Figure 1.1 : The TIVA for regulating anesthesia states [26].

opportunities for control engineers. The control diagram of the patient's hypnotic state can be diagrammed as seen in Figure 1.2.

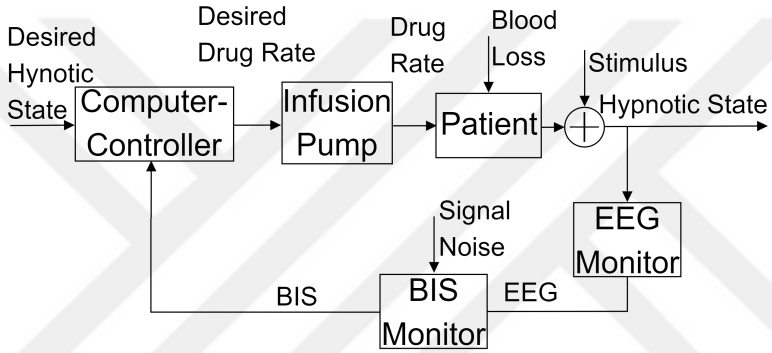

Figure 1.2 : The control diagram of the patient's hypnotic state.

1.1 Literature Review

Control of anesthetic processes and automation of anesthesia are among the top problems that academic studies and engineering applications have focused on in biomedical engineering. The main reason for that hard work on automatic control of anesthesia is the requirement of anesthesiologists to manage a greater volume of intricate tasks after the advancements in medical technology that have led to an escalation in the complexity of surgical procedures [27]. Moreover, due to an insufficient understanding of anesthesia's underlying mechanisms and significant variations between patients, conventional control frameworks have not produced satisfactory results in a clinical setting [13]. The automation of anesthesia offers improved performance, safety, efficiency, and intra-&inter-patient robustness.

One of the first uses of infusion-controlled TIVA using micro-controllers and 3 compartmental models occurred in 1988. According to patient models, it used an open-loop algorithm to achieve pre-determined blood concentrations varying between $3,24 - 4.07 \mu g/ml$. The induction phase was planned to take 2 minutes, and the maintenance phase would take nearly 90 minutes while maintaining the blood levels constant. Within a minute, all patients experienced a loss of consciousness, and no complaints of arm pain were reported [28].

Compared to the manual administration methods, the control strategies for TIVA mostly aimed to improve the outcomes in terms of performance, robustness, and disturbance rejection. Different methods of controlling anesthesia have been studied to achieve this; the most common are PID control, MPC, and adaptive control [8]. Despite promising results, automatic control systems aren't commonly used in clinical practice frequently [29].

An early example of CL-TIVA was conducted in 1999. The BIS of a group of patients whose average age is 41 and the average weight is 60 kilograms has been controlled near BIS of $55(44 - 64)$ for an average of 87 minutes. An altered version of the PID controller structure was used as the system's controller in parallel with manual open-loop control. Similar outcomes in administering anesthesia were observed using closed-loop and manual control methods. Interoperate conditions and recovery characteristics were comparable between the two methods. No significant differences were found in cardiovascular and electroencephalographic variables during anesthesia maintenance [30].

A clinical assessment was conducted on nearly a hundred children using PID-TIVA in [31]. The controller gains have been calculated to achieve sufficient robustness margins for the uncertainty identified according to a group of models that explains the differences between patients. The assessment has resulted in proven PID-TIVA viability for induction and maintenance phases using robust parameter tuning to accommodate the inter-patient variability [31]. Robust PID-TIVA structures are also studied in [32] for analyzing better performance limitations. An evaluation of the PID-TIVA controller whose parameters have been calculated using optimization

techniques has been presented in [7]. The proposed system in this study has the ability to handle both the induction and maintenance phases automatically by scheduling two sets of controller gains. The results were obtained from 5 male and 5 female plastic surgery patients whose ages varied between 39-88. Loss of consciousness has been induced and maintained successfully for all patients without any interventions [7]. Moreover, a modified PID-TIVA with an artificial appropriate bolus during induction alongside a nonzero baseline infusion during the maintenance phase structure has been introduced and tested experimentally in [33].

MPC-TIVA is also feasible for closed-loop control of hypnotic states of anesthesia. The performance of a general predictive control strategy in drug dosage control with an anesthesia-specific control algorithm has been examined, and the robustness properties of the prediction-based controller have been evaluated concerning variability between different patients and over time within the same patient in [34]. Moreover, the limitations of MPC-TIVA strategies have been investigated, and a safety system has been formalized with the constraints in [35].

Adaptive control means the controller updates its control law to adapt to changing conditions over time, which implies inter-patient adaptability and operability for intra- and inter-patient CL-TIVA [8]. An individualized PID-TIVA structure with patient model identification using a gradient-based identification method is presented in [36]. The simulations using 44 patient models improved load and uncertainty compensation performance [36]. An EPSAC-TIVA scheme, an indirect adaptive MPC that uses parameter estimation methods with LSE for control of depth of anesthesia, has been introduced in [37]. The EPSAC-TIVA has been updated to compensate for inter-patient uncertainties with an online gain adaptation method based on changing the control target between the induction and maintenance phases. The results of this controller performed properly on simulations for 12 patient models [38].

1.2 Purpose of Thesis

The TIVA system is considered one of the systems with the most time-variant features, intra-patient and inter-patient differences, unpredictability, and model uncertainty in control systems. It has been stated that closed-loop control of anesthesia is far

harder than aviation systems, which are defined by certain psychic laws, include well-defined parameters, and inputs-outputs are mostly measurable [39]. The dynamics of consciousness are mostly unknown and difficult to model in anesthesia [40]. Controlling anesthesia presents numerous challenges, including variability among patients and within patients themselves, multiple variables to consider, varying time delays, dynamics that depend on the type of hypnotic agent used, and stability concerns [30,37,41].

Compartmental models, which represent drug distributions in body tissues, are frequently used in control system design for TIVA. An additional nonlinear filter is added to the output of compartmental TIVA models to represent the patient's hypnotic states and unconsciousness. These are the most common models for TIVA in the literature and are considered one of the best representations of hypnotic states mathematically. These models can be improved using output delays in both compartmental models and nonlinear filters.

Despite the variety of control systems developed, such as PID control, MPC, and various adaptive control methods, the inability to provide intra-patient and inter-patient validity is one of the biggest obstacles to applying anesthesia systems with automatic control features to larger patient groups. Therefore, new adaptive control structures are required that provide intra-patient and inter-patient validity, easy implementation, robust operations, and require the least amount of patient parameter dependency.

One of the main goals of this thesis is to suggest a method to improve common TIVA models with additional output delays using real surgical patient data. These improved models are expected to produce more correlation between real and simulated outputs of the same patient models. Moreover, this thesis suggests an adaptive controller structure for CL-TIVA that produces better results such as robustness than common PID-TIVA controllers for intra- and inter-patient operations. The suggested controller is a model reference adaptive controller that adaptation laws are generated by the Lyapunov's theory. This MRAC controller is expected to produce lower integral-absolute-error values than classical PID-TIVA structures while the effect of blood loss and stimuli disturbances persist.

1.3 Thesis Outline

The thesis is structured as follows: After the Introduction chapter, where TIVA systems are introduced, the literature review is shared, and the purpose of the thesis is explained, chapter two delves into the total intravenous anesthesia model, beginning with compartmental modeling and then analyzing the pharmacokinetic-pharmacodynamic patient model. This section also explores the effects of blood loss and other disturbances. It further investigates patient databases, emphasizing linear patient model identification from surgical data and approximating the Hill curve using least squares error analysis. The chapter concludes with an examination of the delayed patient model.

Chapter three addresses inter-patient control of anesthesia by outlining key performance criteria and limitations. It discusses PID control and Lyapunov-based Model Reference Adaptive System (MRAS) design, encompassing an observer-based state feedback control system focusing specifically on state feedback controller design and observer design. The chapter also provides an in-depth analysis of the model reference adaptive controller, covering its reference model and Lyapunov's theory, culminating in applying these concepts to intravenous anesthesia. This section concludes with a comparative analysis of patient database results. The thesis concludes with a Conclusion chapter.

2. TOTAL INTRAVENOUS ANESTHESIA MODEL

A critical element in understanding the response of the human body to drug administration, particularly emphasized in disciplines like anesthesiology, is the mathematical description of such responses, allowing for the prediction of patient reactions to drug boluses during anesthesia induction and continuous infusions for maintenance [2]. Therefore, mathematical models and differential equations representing the dynamics of drug distributions for patients need to be obtained in order to control anesthetic processes and automate anesthesia.

This chapter explains the intravenous anesthesia model, starting with the modeling method called compartmental modeling, and deriving its differential equations and parameters. After that, it explains the common anesthesia model that contains a three-compartmental pharmacokinetic model and a one-compartmental pharmacodynamic model alongside the Hill curve, which acts like a nonlinear output gain and considers the effect of blood loss during surgery. It introduces the extended delayed patient model, which considers time delays in model states for single and multiple-state cases. Finally, it explains the common patient databases and shares the analysis results for different patients in terms of pole-zero distributions, controllability, and observability.

2.1 Compartmental Modelling

Control of biomedical systems requires an administrated drug input, mostly as an intravenous injection where the drug is injected into the body. In such cases, the periodic movement of the heart mixes the drug with the blood and distributes the drug evenly to the body after it enters the circulatory system [42]. The diffusion of the drug to the different tissues of the body can be modeled with compartments using different diffusion rates between neighboring tissues. Therefore, compartmental modeling is

a useful method that produces linear pharmacokinetic models for modeling the drug distribution dynamics in the human circulatory system [42].

Compartmental modeling, which elucidates the transfer of substances between different compartments, finds its roots in investigations of tracer-labeled compound metabolism during the 1920s [43]. Compartmental modeling is mostly concerned with the concentration of drugs in tissue which is described by Fick's Law of diffusion which describes the process of the movement of a drug solute between two compartments that are separated by a thin membrane as seen in Equation 2.1 [43], [44].

$$\frac{dq}{dt} = -D_q A_q \frac{dc_q}{dx_q} \tag{2.1}$$

Equation 2.1 describes the relationship between various parameters involved in solute diffusion across a membrane by Fick's Law of Diffusion. In this equation, q represents the quantity of solute, A_q denotes the membrane surface area, c_q signifies the concentration of the solute, D_q stands for the diffusion coefficient, dx_q represents the membrane thickness, and $\frac{dc_q}{dx_q}$ indicates the concentration gradient.

The membrane thickness dx_q can be approximated to Δx_q, which turns the concentration gradient $\frac{dc_q}{dx_q}$ into $\frac{c_{q_1} - c_{q_2}}{\Delta x_q}$ for two compartmental models where c_{q_1} and c_{q_2} represents the concentration of first and second compartments respectively. The Equation 2.1 can be rewritten as seen in Equation 2.2.

$$\frac{dq_1}{dt} = -D_q A_q \frac{c_{q_1} - c_{q_2}}{\Delta x_q} \tag{2.2}$$

Considering that $q_1 = c_{q_1} V_{q_1}$ and $\dot{q_1} = \dot{c_{q_1}} V_{q_1}$, Equation 2.2 can be re-written as seen in the Equation 2.3.

$$V_1 \frac{dc_{q_1}}{dt} = -\frac{D_q A_q}{\Delta x_q} \left(c_{q_1} - c_{q_2} \right) \tag{2.3}$$

A flow transfer rate parameter K_q can be defined as seen in Equation 2.4.

$$K_q = \frac{D_q A_q}{\Delta x_q} \tag{2.4}$$

Equation 2.3 can be rewritten using Equation 2.4 as seen in Equation 2.5.

$$\frac{dc_{q_1}}{dt} = -\frac{K_q}{V_{q_1}}\left(c_{q_1} - c_{q_2}\right) \tag{2.5}$$

It is possible to state that a compartmental system with N compartments can be modeled with N first order ODEs and N states [45]. Inputs of these systems can be defined as a bolus injection, which is an immediate injection of a solute into a compartment that acts like an impulse, and constant continuous injection, which is delivered by an infusion pump or an intravenous drip into a compartment that acts like a step input [43]. A 2-compartmental model diagram with external solute input and output is seen in Figure 2.1.

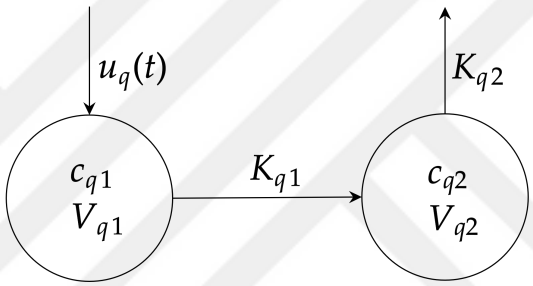

Figure 2.1 : 2 compartmental solute concentration system with external input and output.

$$\frac{dc_{q_1}}{dt} = u_q(t) - \frac{K_{q_1}}{V_{q_1}}c_{q_1}(t) \tag{2.6}$$

$$\frac{dc_{q_2}}{dt} = \frac{K_{q_1}}{V_{q_1}}c_{q_1}(t) - \frac{K_{q_2}}{V_{q_2}}c_{q_2}(t) \tag{2.7}$$

Equations 2.6 and 2.7 are the pair of ODEs that represent the dynamical model of the system shown in Figure 2.1. Here $\frac{dc_{q_1}}{dt}$ and $\frac{dc_{q_2}}{dt}$ are in terms of milligrams per minute, c_{q_1} and c_{q_2} are in milligrams, K_{q_1} and K_{q_2} are in liters per minute, V_{q_1} and V_{q_2} are in liters, $u_q(t)$ is in miligrams per minute. If $K_{q_1} = 2L/min$, $K_{q_2} = 4L/min$, $V_{q_1} = 1L$, and $V_{q_2} = 2L$, the $c_{q_1}(t)$ and $c_{q_2}(t)$ obtains as seen in the Figures 2.2 and 2.3 for constant continuous infusion input and bolus injection input respectively.

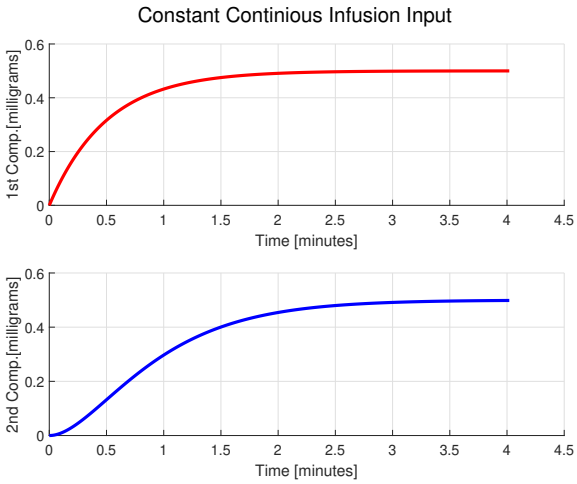

Figure 2.2 : Simulation results for constant continuous infusion input for given system.

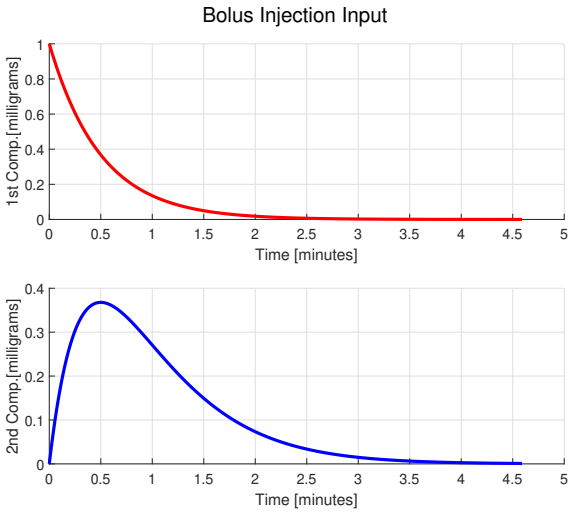

Figure 2.3 : Simulation results for bolus injection input for given system.

Figures 2.2 and 2.3 show that it is possible to get an equilibrium point for drug levels in compartments. Precise compartmental pharmacokinetic models are valuable for crafting closed-loop drug delivery systems. These systems aim to regulate drug concentration within a compartment, ensuring it stays within specified upper and lower bounds for optimal efficacy and minimal side effects [42].

2.2 Pharmacokinetical-Pharmacodynamical Patient Model

One particular way to model the anesthetic drug distributions that produce successful results is compartment modeling and compartment analysis [42]. Patient

compartment models for anesthesia mostly consist of pharmacokinetics (PK) and pharmacodynamics (PD) blocks where PK defines the drug concentrations in intravascular blood and fat-muscle sub-biological systems, and PD defines the effects of the drug concentration in the blood system on the patient [46]. PK and PD models can be cascaded into each other as a combination of a linear part and a static nonlinearity as seen with block diagrams in Figure 2.4 [47].

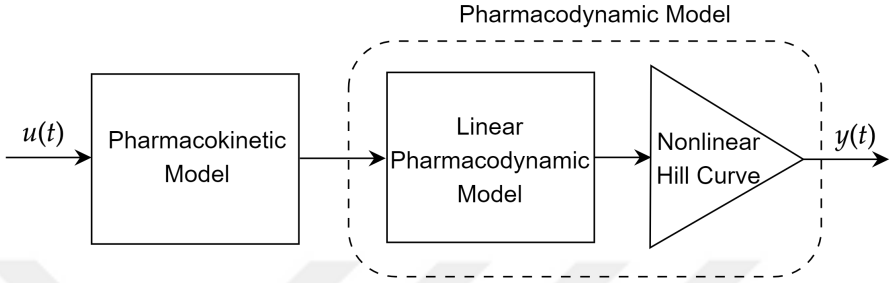

Figure 2.4 : Pharmacokinetical-pharmacodynamical model.

The system seen in the Figure 2.4 is a Wiener-Hammerstein model which is common in modeling and control of anesthetic processes [46], [48]. The pharmacokinetical model can be considered as a 3 compartmental mammillary model. In such a mammillary model, the central compartment facilitates the exchange of material with two peripheral compartments, wherein the peripheral compartments exclusively interact with the central compartment and do not exchange material with each other [42], [45]. The pharmacodynamical model is a combination of a linear 1-compartmental model corresponding to 1 linear ODE, which takes the output of the pharmacokinetic side as input, and the Hill curve filter output, which can be considered as a nonlinear static gain. The whole system can be considered as a 4^{th} order compartmental system with nonlinear gain, and its diagram is as seen in Figure [49], [50], [51], [52].

The drug input $u(t)$ is the propofol input in terms of milligrams per milliliters per minute $(mg/ml/min)$. The central compartment of the system is the fast compartment that represents blood. $x_1(t)$ is the drug concentration in blood in terms of milligrams of drug per milliliter. 1^{st} and 2^{nd} peripheral compartments represent the slow compartments where they can be considered as muscle and fat tissue, respectively. $x_2(t)$ and $x_3(t)$ states represent the drug concentrations in terms of milligrams of milliliters in muscle and fat tissue, respectively. Moreover, K_{ij} represents the drug

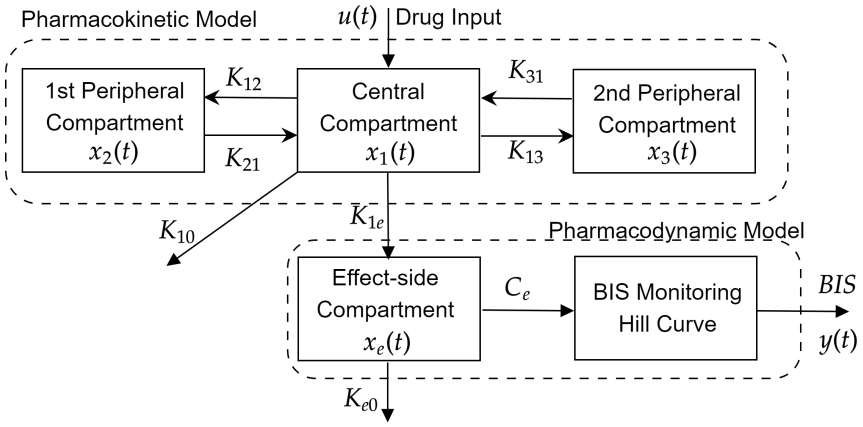

Figure 2.5 : The diagram of 4 compartmental model.

transfer rates where i is the source, j is the destination and i is not equal to j for all time [52].

The effect side compartment is a hypothetical compartment where $x_e(t)$ represents the effective concentration of drug in the cerebral cortex [2], [46]. The measurable output of this system $y(t)$ is the Bispectral Index (BIS) value which requires a monitoring process. The bispectral analysis defines a value that differs between 0 and 100 from the frequency phase relationships of sinusoidal components of EEG signals [53]. The monitoring results from dose to effect can be approximated into a nonlinear hill curve which is a suitable representation for dose-effect monitoring [52], [54]. The differential equations for a linear part, the 4 compartmental PK-PD model without the nonlinear Hill curve gain, can be obtained in accordance with the presented compartmental modeling methods as seen in Equation 2.8.

$$\begin{aligned}
\dot{x}_1(t) &= -[k_{10}+k_{12}+k_{13}]\cdot x_1(t)+k_{21}\cdot x_2(t)+k_{31}\cdot x_3(t)+\frac{u(t)}{V_1}\\
\dot{x}_2(t) &= k_{12}\cdot x_1(t)-k_{21}\cdot x_2(t)\\
\dot{x}_3(t) &= k_{13}\cdot x_1(t)-k_{31}\cdot x_3(t)\\
\dot{x}_e(t) &= -k_{e0}\cdot x_e(t)+k_{1e}\cdot x_1(t)
\end{aligned} \tag{2.8}$$

The parameters k_{ij} are dependent on age, lean body mass (LBM), and hence weight, and gender. These intermediate parameters can be calculated as seen in the Equations 2.9 and 2.10.

$$
\begin{aligned}
lbm_{Male} &= 1.1 \cdot weight - 128 \frac{weight^2}{height^2} \\
lbm_{Female} &= 1.07 \cdot weight - 148 \frac{weight^2}{height^2}
\end{aligned}
\tag{2.9}
$$

$$
\begin{aligned}
V_1 &= 4.27\,[L] \\
V_2 &= 18.9 - 0.391 \cdot (age - 53)\,[L] \\
V_3 &= 2.38\,[L] \\
C_{l1} &= 1.89 + 0.456(weight - 77) - 0.0681(lbm - 59) \\
&+ 0.264(height - 177)\,[L/min] \\
C_{l2} &= 1.29 - 0.024 \cdot (age - 53)\,[L/min] \\
C_{l3} &= 0.836\,[L/min]
\end{aligned}
\tag{2.10}
$$

C_{l1} represents the rate at which the drug is eliminated from the body, while C_{l2} and C_{l3} denote the rates at which the drug is transferred from the central compartment to two peripheral compartments [46]. The parameters k_{ij} can be calculated using C_{l1}, C_{l2}, C_{l3} as seen in the Equation 2.11 and these parameters are in terms of $[min^{-1}]$. The parameters and the model can be converted into $[s^{-1}]$ by dividing the parameters by 60.

$$
\begin{aligned}
k_{10} &= \frac{C_{l1}}{V_1}\,[\,\mathrm{min}^{-1}] \\
k_{12} &= \frac{C_{l2}}{V_1}[\,\mathrm{min}^{-1}] \\
k_{13} &= \frac{C_{l3}}{V_1}[\,\mathrm{min}^{-1}] \\
k_{21} &= \frac{C_{l2}}{V_2}[\,\mathrm{min}^{-1}] \\
k_{31} &= \frac{C_{l3}}{V_3}[\,\mathrm{min}^{-1}] \\
k_{e0} &= 0.456[\,\mathrm{min}^{-1}]
\end{aligned}
\tag{2.11}
$$

The mathematical model of the linear part of the system in state space form can be obtained using the differential equations given in the Equation 2.8 and k_{ij} parameters as seen in the Equation 2.12.

$$\begin{bmatrix} \dot{x}_1 \\ \dot{x}_2 \\ \dot{x}_3 \\ \dot{x}_e \end{bmatrix} = \begin{bmatrix} -(k_{10}+k_{12}+k_{13}) & k_{21} & k_{31} & 0 \\ k_{12} & -k_{21} & 0 & 0 \\ k_{13} & 0 & -k_{31} & 0 \\ k_{1e} & 0 & 0 & -k_{e0} \end{bmatrix} \begin{bmatrix} x_1 \\ x_2 \\ x_3 \\ x_e \end{bmatrix} + \begin{bmatrix} 1 \\ 0 \\ 0 \\ 0 \end{bmatrix} u(t)$$

$$y = \begin{bmatrix} 0 & 0 & 0 & 1 \end{bmatrix} \begin{bmatrix} x_1 \\ x_2 \\ x_3 \\ x_e \end{bmatrix} \tag{2.12}$$

The output of this state space model is clearly $x_e(t)$, which is the effect-side concentration in terms of $[mg/ml]$. The nonlinear part of the pharmacodynamical model can be integrated into the model as a filter that takes $x_e(t)$ as an input and produces BIS output with the Hill curve. The nonlinear static function Hill curve for BIS monitoring is as seen in Equation 2.13.

$$E = E_0 - \frac{E_{\max} \cdot x_e^{\gamma}}{C_{50}^{\gamma} + x_e^{\gamma}} \tag{2.13}$$

E_0 defines the maximum value of BIS, which is the awake state as 100, and E_{max} defines the minimum value of BIS. C_{50} is the concentration needed to obtain %50 of the maximum effect. γ determines the steepness of the Hill curve. Here, E_{max} and γ is the Hill-coefficient varies between the patients.

One of the main problems in the control of anesthesia is the inability to measure the states, which are defined as drug concentrations in effect-side, blood, fat, and muscles, where most of the linear control methods at least require the effect-side concentration. One way to obtain the effect-side concentration is to use the inverse of the Hill curve, which takes measurable BIS value as input and calculates the effect-side concentration. The Hill nonlinearity varies monotonically with the normalized CE. As a result, an inverse relationship is established between them as seen in Equation 2.14 [46].

$$C_e(t) = \mathrm{C}_{50} \left(\frac{E_0 - \mathrm{BIS}(t)}{E_{\max} - E_0 + \mathrm{BIS}(t)} \right)^{\frac{1}{\gamma}} \tag{2.14}$$

2.3 Blood Loss Effect and Disturbances

It is possible to mention a change in the body fluid, which is mostly caused by blood losses during the surgeries [55], [56]. The blood volume is represented as V_1 in the Equation 2.10. It is possible to state that a change in the blood volume V_1 will also cause a change in the parameters k_{10}, k_{12} and k_{13} as seen the Equation 2.11 alongside with the change in drug input $u(t)/V_1$ as seen in the Equation 2.8. Therefore, these parameters can be considered as time-variant while the blood volume changes over time because of the hemorrhage during the surgery. The state space model in the blood loss change case can be rewritten as seen in the Equations 2.15 and 2.16.

$$\begin{aligned} \dot{x}(t) &= A(t)\cdot x(t) + B(t)\cdot u(t) \\ y(t) &= C\cdot x(t) \end{aligned} \tag{2.15}$$

$$\begin{bmatrix} \dot{x}_1 \\ \dot{x}_2 \\ \dot{x}_3 \\ \dot{x}_e \end{bmatrix} = \begin{bmatrix} -(k_{10}(t)+k_{12}(t)+k_{13}(t)) & k_{21} & k_{31} & 0 \\ k_{12}(t) & -k_{21} & 0 & 0 \\ k_{13}(t) & 0 & -k_{31} & 0 \\ k_{1e} & 0 & 0 & -k_{e0} \end{bmatrix} \begin{bmatrix} x_1 \\ x_2 \\ x_3 \\ x_e \end{bmatrix} + \begin{bmatrix} \frac{1}{V_1(t)} \\ 0 \\ 0 \\ 0 \end{bmatrix} u(t)$$

$$y = \begin{bmatrix} 0 & 0 & 0 & 1 \end{bmatrix} \begin{bmatrix} x_1 \\ x_2 \\ x_3 \\ x_e \end{bmatrix} \tag{2.16}$$

The effect of the blood loss can be simulated by decreasing the volume of the central compartment V_1 from $4,27[L]$ to $3[L]$ using step or ramp signal profiles in 1000 seconds [56]. The $V_1(t)$ can be written as seen in the Equation 2.17 in step profile case and can be written as seen in the Equation 2.18 in ramp profile case [56]. The values t_1, t_2, and t_3 represent the times when the hemorrhage occurs and the volume of the central compartment changes.

$$V_1(t) = \begin{cases} 4,27; & t < t_1 \\ 4; & t_1 < t_2 < t_2 \\ 3,75; & t_2 < t_3 < t_3 \\ 3; & t > t_3 \end{cases} \tag{2.17}$$

$$V_1(t) = \begin{cases} 4,27; & t < t_1 \\ \frac{-1.27}{100} \cdot (t - t_1) + 4,27; & t_1 \leqslant t < t_1 + 1000 \\ 3; & t \geqslant t_1 + 1000 \end{cases} \tag{2.18}$$

Disturbances occur as stimulations in addition to the blood loss during the surgery [46]. Such stimulations are considered to happen during the maintenance phase of the anesthesia process [57]. A typical disturbance profile in terms of ΔBIS is as seen in Figure 2.6. Such disturbances and the effect of blood loss are expected to be canceled out by the controller during the closed-loop anesthesia process.

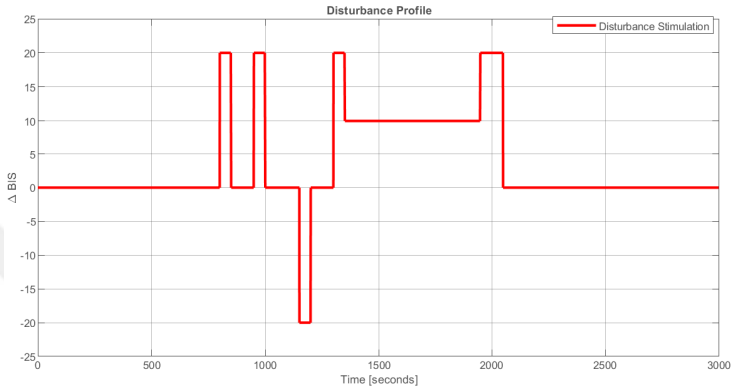

Figure 2.6 : Disturbance Profile.

2.4 Patient Databases

It is possible to sum up from Equations 2.9, 2.10 and 2.13 that the patient model is dependent on age, height, weight, gender, C_{50}, E_{50} and γ parameters of the patients. It is important to use real patient databases in control design for anesthesia in order to get the most realistic results. A patient database for 24 patients has been used in this study [52]. The database is as seen in the Table A.1 in Appendix A.

The model of each patient has 4 poles and 2 zeros on the left, stable side of the complex plane. The pole-zero distribution for the database is as seen in Figure 2.7. Here, the blue x markers represent the pole locations, while the red o markers represent the zero locations. The pole-zero pair closest to the origin is as seen in Figure 2.8.

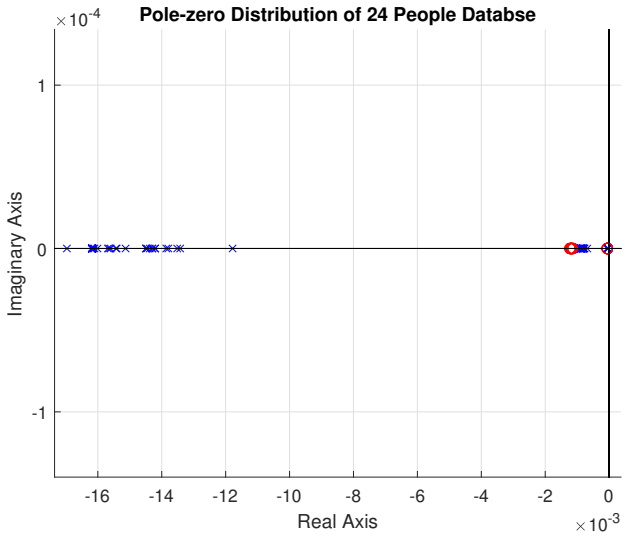

Figure 2.7 : Pole-zero distribution of 24 people database.

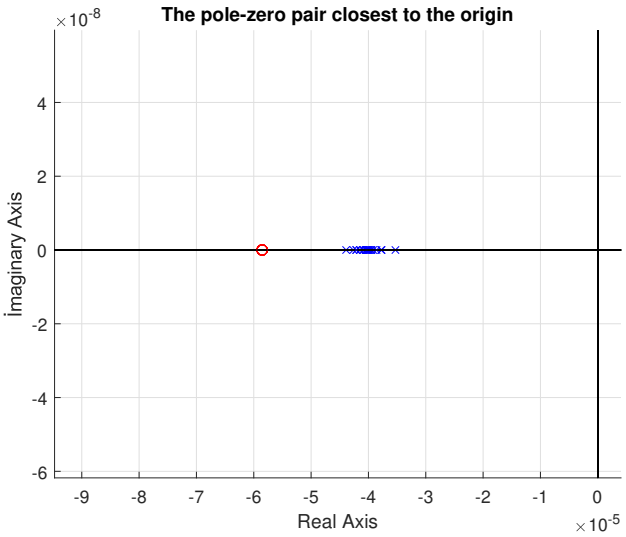

Figure 2.8 : The pole-zero pair closest to the origin.

It is possible to say from 2.8 that even though the poles are close to the origin, they do not pass through to the right half side of the complex plane for the data of 24 patients.

A set of patient parameters considered as the nominal patient is required for control design and prediction purposes [58], [59]. The nominal patient parameters can be calculated by taking the average values of the patient parameters from the data of 24 people. The nominal patient parameters are as seen in Table 2.1.

Table 2.1 : Parameters of Nominal Patient

Patient	**Age**	**Height**	**Weight**	C_{50}	γ
Nominal	65.1667	172.875	83.125	4.1821	2.4646

The state space matrices in Equation 2.12 can be obtained for nominal patients as seen in Equation 2.19. Moreover, the pole-zero map of the nominal patient is as seen in Figure 2.9.

$$\begin{aligned}
\mathbf{A}_{\mathrm{p}} &= \begin{bmatrix} -0.0144 & 0.0012 & 0.0001 & 0 \\ 0.0039 & -0.0012 & 0 & 0 \\ 0.0033 & 0 & -0.0001 & 0 \\ 0.0076 & 0 & 0 & -0.0162 \end{bmatrix} \\
\mathbf{B}_{\mathrm{p}} &= \begin{bmatrix} 0.2342 \\ 0 \\ 0 \\ 0 \end{bmatrix} \\
\mathbf{C}_{\mathrm{p}} &= \begin{bmatrix} 0 & 0 & 0 & 1 \end{bmatrix} \\
\mathbf{D}_{\mathrm{p}} &= \begin{bmatrix} 0 \end{bmatrix}
\end{aligned} \tag{2.19}$$

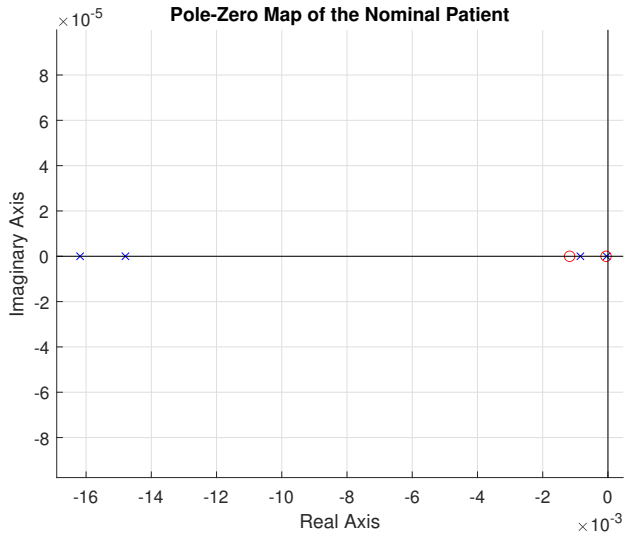

Figure 2.9 : Pole-zero map of the nominal patient.

The VitalDB database, which is a common database for cardiovascular simulations [60] and anesthetic deep learning frameworks [61], have been used in order to obtain real patient surgical data and improve the results alongside the patient data given in Table 2.1. VitalDB is an open-access database with 6388 recordings that include vital surgical signals such as electrocardiography, blood pressure, percutaneous oxygen

saturation, and body temperature of real surgical patients [62]. VitalDB also includes processed anesthesia data in order to monitor BIS, effect-site concentration, and drug administrations. Drug input rate, effect-site concentration, and BIS output of a patient from VitalDB as seen in Figure 2.10. The sample time of the data is 1 second.

Surgical data for a total of 11 patients were retrieved from VitalDB for subsequent identification studies. These patients have been chosen according to the criteria of stable BIS signal [63]. The data taken from VitalDB include NaN values, which would disturb data analysis processes. Therefore, data cleaning pre-processes have been run to get rid of non-usable data.

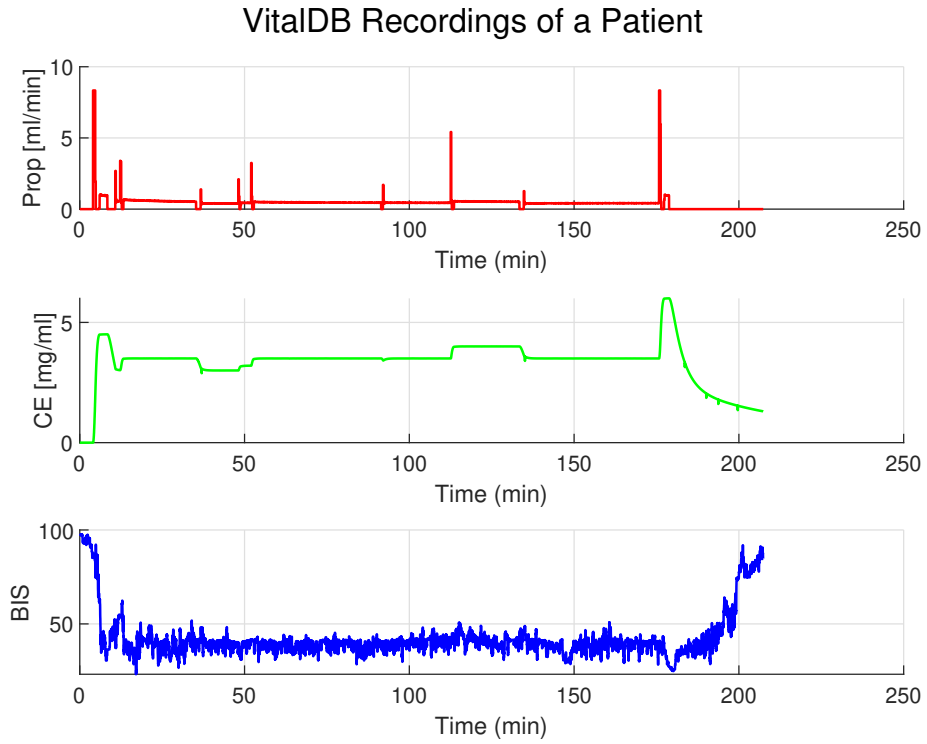

Figure 2.10 : VitalDB recordings of a patient.

2.4.1 Linear Patient Model Identification from Surgical Patient Data

It is possible to identify linear models of the patients and find a linear approximation of a nonlinear hill curve using the least squares error method using this data. The LSE formula is as seen in Equation 2.20.

$$y(t) = \varphi^{\mathrm{T}}(t)\theta \tag{2.20}$$

Here $y(t)$ represents the measurable output, $\varphi^{\mathrm{T}}(t)$ is the regressors which are known data, and θ is the vector of unknown parameters which are desired to be identified. If there the data is offline and collected before, the θ parameter vector can be calculated as seen in the Equation

$$\theta = \left(\varphi^T \varphi\right)^{-1} \varphi^T Y \tag{2.21}$$

The parametric discrete-time transfer function model for 1 second of sampling time of the linear patient model can be written as seen in Equation 2.22. The aim of the identification is to find $n_3, n_2, n_1, n_0, d_3, d_2, d_1$ and d_0 parameters of this model. An ARX model structure has been constructed in order to identify the linear model between propofol rate input and effect-side concentration from the data in the database in order to obtain regressor and parameter vectors. The ARX model is as seen in Equation 2.23. Here $q = z^-1$.

$$G(z) = \frac{\left(n_3 \cdot z^3 + n_2 \cdot z^2 + n_1 \cdot z^1 + n_0 \cdot z^0\right)}{\left(z^4 + d_3 \cdot z^3 + d_2 \cdot z^2 + d_1 \cdot z^1 + d_0 \cdot z^0\right)} \tag{2.22}$$

$$\begin{aligned} A\left(q^{-1}\right) y(k) &= B\left(q^{-1}\right) u(k) + e(k) \\ A\left(q^{-1}\right) &= \left(1 + d_3 \cdot q^1 + d_2 q^2 + d_1 q^3 + d_0 q^4\right) \\ B\left(q^{-1}\right) &= \left(n_3 q^1 + n_2 q^2 + n_1 q^3 + n_0 q^4\right) \end{aligned} \tag{2.23}$$

The ARX model given in Equation 2.23 can be rewritten as seen in Equation 2.24.

$$\begin{aligned} y(k) = &-d_3 y(k-1) - d_2 y(k-2) - d_1 y(k-3) - d_0 y(k-4) \\ &+ n_3 u(k-1) + n_2 u(k-2) + n_1 u(k-3) + n_0 u(k-4) \end{aligned} \tag{2.24}$$

The regression and parameter vectors can be constructed as seen in Equation 2.25.

$$\varphi = \begin{bmatrix} -y(k-1) \\ -y(k-2) \\ -y(k-3) \\ -y(k-4) \\ u(k-1) \\ u(k-2) \\ u(k-3) \\ u(k-4) \end{bmatrix} \quad \hat{\theta} = \begin{bmatrix} -d_3 \\ -d_2 \\ -d_1 \\ -d_0 \\ n_3 \\ n_2 \\ n_1 \\ n_0 \end{bmatrix} \tag{2.25}$$

The identified model output as effect-side concentration for the patient whose data is as seen in Figure 2.10 together with the real effect-site concentration is as seen in Figure 2.11. The identified model output for effect-side concentration for all 11 patients is as seen in Figure A.1 in Appendix A.

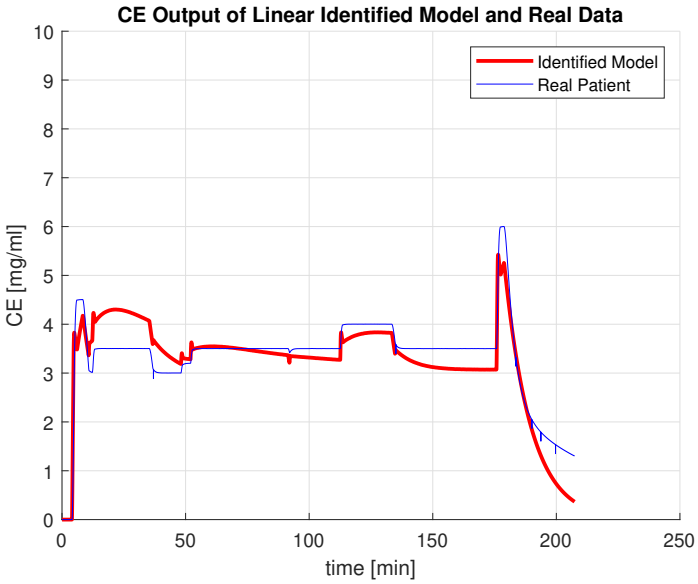

Figure 2.11 : The identified model output.

2.4.2 Approximation of Hill Curve Using Least Square Errors

The nonlinear Hill curve given in Equation 2.13 can be approximated into a first-order shifted linear function using the surgical patient data of CE and BIS. The relation between CE and BIS as a first-order shifted linear function can be written as seen in Equation 2.26 [38].

$$y(t) = k_h \cdot x(t) + d_h \tag{2.26}$$

Here k_h represents the slope of the function, and d_h is the shift offset. The least squares error method and calculation of the unknown parameter vector is similar to Equations 2.20 and 2.21. The regression and parameter for hill curve approximation using least squares are as seen in Equation 2.27.

$$\varphi = \begin{bmatrix} u(k) \\ 1 \end{bmatrix} \quad \hat{\theta} = \begin{bmatrix} k_h \\ d_h \end{bmatrix} \tag{2.27}$$

Here $u(k)$ is the effect-side concentration CE. The 1st order shifted linear function that represents the approximated hill function is obtained for all 11 patients, and the parameters are as seen in Table 2.2.

Table 2.2 : The 1st order shifted linear function parameters for surgical patients.

Patient	k_h	d_h
1	-10.5940	77.7156
2	-6.2348	51.6188
3	-7.9070	71.8244
4	-10.6418	72.7630
5	-8.9506	71.8791
6	-11.9614	74.4970
7	-12.9104	85.9719
8	-10.0038	78.8882
9	-14.4485	81.6383
10	-14.4986	78.3749
11	-6.0544	63.9599

The comparison between the first patient's real BIS data and approximated BIS data, which takes real CE data as input, is as seen in Figure 2.12.

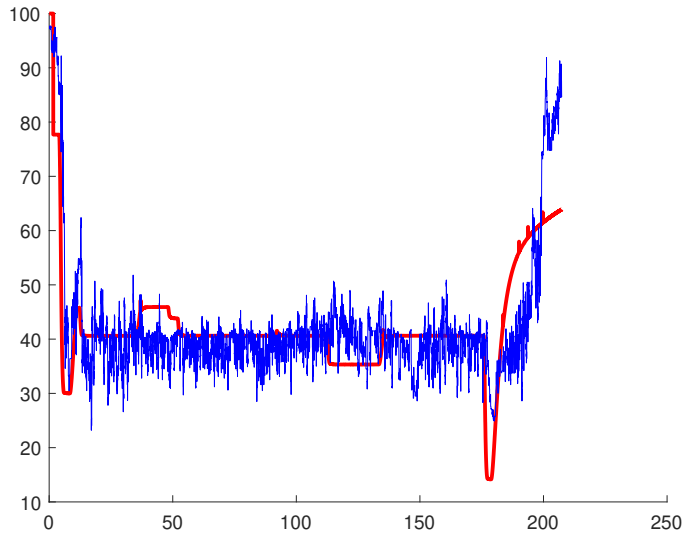

Figure 2.12 : The comparison between the first patient's real BIS data and approximated BIS data from real CE data.

It is possible to say from Figure 2.12 that the approximated hill curve has followed the real BIS data if noise is considered to be canceled. The final model can be constructed

as seen in Equation 2.28 when the identified linear patient model and approximated hill curve function are combined with each other cascade.

$$\begin{aligned} \dot{x}(t) &= A_p \cdot x(t) + B_p \cdot u(t) \\ y(t) &= k_h \cdot C_p \cdot x(t) + d_h(t) \end{aligned} \tag{2.28}$$

The function $d_h(t)$ is the output offset function where its value equals 100 initially; then, it equals the shift offset obtained from LSE. The identified model as seen in the Equation 2.28 has been obtained as seen in the Equation 2.29 when the matrices written in controllable canonical form.

$$\begin{bmatrix} \dot{z}_1 \\ \dot{z}_2 \\ \dot{z}_3 \\ \dot{z}_4 \end{bmatrix} = \begin{bmatrix} 0.9498 & 0.3182 & 0.0813 & -0.3497 \\ 1.0000 & 0 & 0 & 0 \\ 0 & 1.0000 & 0 & 0 \\ 0 & 0 & 1.0000 & 0 \end{bmatrix} \begin{bmatrix} z_1 \\ z_2 \\ z_3 \\ z_4 \end{bmatrix} + \begin{bmatrix} 1 \\ 0 \\ 0 \\ 0 \end{bmatrix} u(t)$$

$$y = 10^{-3} \cdot \begin{bmatrix} 0.0446 & 0.0045 & -0.0959 & -0.4527 \end{bmatrix} \begin{bmatrix} z_1 \\ z_2 \\ z_3 \\ z_4 \end{bmatrix} + d_h(t) \tag{2.29}$$

Here z_i represents the states of the model in controllable canonical form. The output offset function $d_h(t)$ can be written as seen in the Equation 2.30.

$$d_h(t) = \begin{cases} 100, t = 0 \\ 77.6894, \text{ Otherwise} \end{cases} \tag{2.30}$$

The model given in Equation 2.29 and the output offset function given in Equation 2.30 have been obtained for all 11 patients in VitalDB. The results and comparison of BIS values for the identified model output of the 1st patient and the real BIS data of the 1st patient is as seen in Figure 2.13. The results and comparison of BIS values for the identified model output of all 11 patients are as seen in Figure A.2 in the Appendix.

Correlation analysis is a useful method for analyzing the relationship between results [64]. The correlation coefficients of the two datasets can be classified as strong negative, weak negative, weak positive, and strong positive correlations as the coefficient takes values between -1 and 1. [65]. The proximity of the correlation coefficient to 1 indicates a high degree of correlation between the data variables,

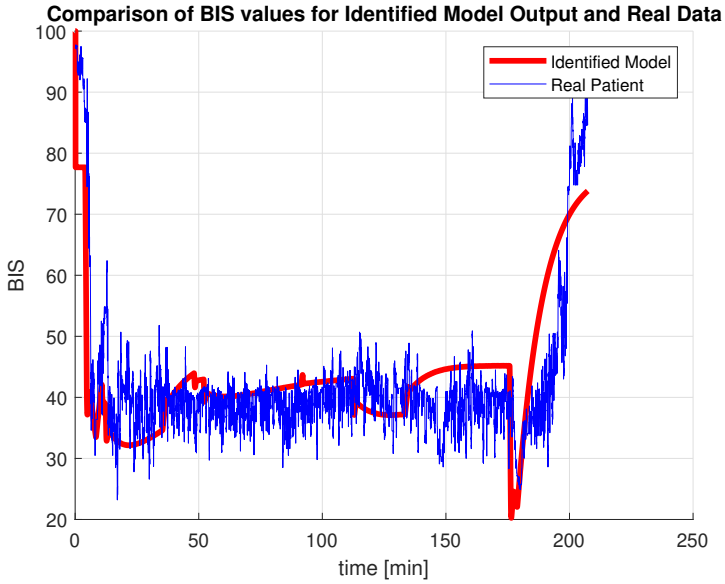

Figure 2.13 : Comparison of BIS values for identified model Output of 1st patient.

suggesting that changes in one variable are strongly associated with corresponding changes in the other [65]. Therefore, correlation analysis between real output data from VitalDB and identified model outputs has been conducted in order to show the correlation of results and viability of identified models. The correlation analysis was conducted for both "Drug Input-CE Output" and "Drug Input-BIS Output" models for each patient. The correlation analysis results are as seen in Figure 2.14 where each bar in the graph represents the correlation coefficient for that patient between real data and identified outputs.

Red bar graphs represent the correlation coefficients between real CE data from VitalDB and CE outputs of identified models of each patient, while blue bar graphs represent the correlation coefficients between real BIS data from VitalDB and BIS outputs of identified models of each patient. It is possible to say from 2.14 that all of the correlation coefficients are higher than 0.7 for CE, which indicates a strong correlation between real and identified model output datasets [66]. All the patients, except for the second patient, have either strong or moderate positive correlation BIS where the interval $0.3 - 0.7$ represents moderate and $0.7 - 1$ represents strong correlation [66]. The average correlation for the CE case is higher than for the BIS case, mostly because of the effect of the monitor noise on BIS data. Moreover, the mean value of the correlation coefficient for a linear patient model with CE output

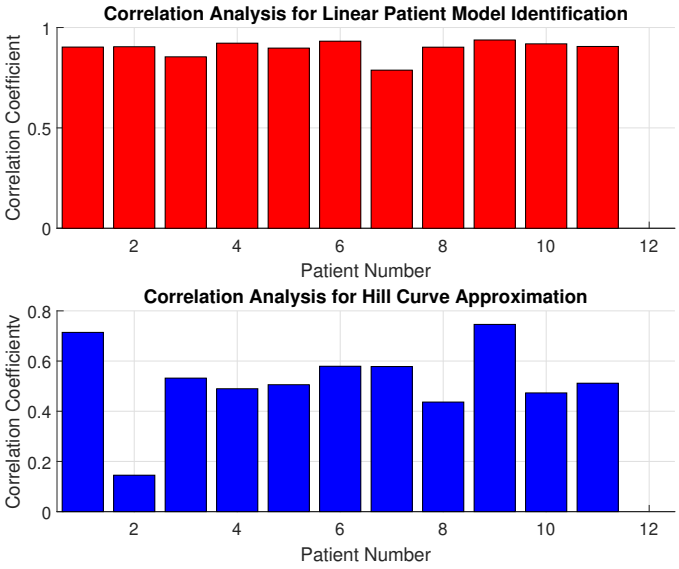

Figure 2.14 : The correlation analysis of LSE results for each patient.

equals 0.896, and the mean value of the correlation coefficient for a linear patient model with BIS output equals 0.512. The mean value of the linear patient model with CE output can considered as a strong correlation to real CE data, while the mean value of the approximated hill curve output has a moderate positive correlation with BIS output.

2.5 Delayed Patient Model

Delays in biological systems typically manifest when alterations over time in a given variable of interest are influenced by the past or historical values of one or more variables that govern the processes of production or elimination [67]. It is possible to say that witnessing a noticeable time lag between the effect of the drug and administration of a drug through a route that does not involve gastrointestinal absorption is common for anesthesiologists [42]. Therefore, it is important to consider time delay stability intervals in controller designs for anesthetic processes which makes delay stability investigation important for real automatic control applications for anesthesia control systems.

The patient models constructed in Equation 2.12 can be modeled with input-output time delays. Possible delays can both occur while the drug is transported to a central compartment on the pharmacokinetic absorption and while the drug is spread from

the central compartment to the effect-site compartment, which is the biophase [68]. Moreover, a monitor time delay, which is mostly between 5 and 10 seconds, related to the manufacturer of the BIS monitor but also depends on the patient parameters, occurs in bispectral index monitoring [69]. The BIS monitoring delay can considered as an output state delay in the delayed patient model. Combining the monitor delay and the biophase delay, the output delays in anesthesia can be between 10 seconds to 30 seconds.

The delayed patient model is suitable to be identified as a linear time-invariant input-output time delay system (LTI-IOTDS) as seen in Equation 2.31. The characteristic equation of this (LTI-IOTDS) system is seen in Equation 2.32.

$$\begin{aligned} \dot{x}(t) &= Ax(t) + Bu(t-\tau_i) \\ y(t) &= C \cdot x(t-\tau_o) \end{aligned} \tag{2.31}$$

$$P_{CE}(s, \tau_m, \tau_b) = \det[s\mathbf{I} - \mathbf{A}] \tag{2.32}$$

The delays on the effect-site compartment represent the biophase delay (τ_b) occurring on the effect-side compartment. The total delay value equals the combination of biophase (τ_b) and BIS monitor delays (τ_m). If the linear PKPD compartmental model described in Equation 2.12 is considered to have a single independent time delay on the output then the model can be constructed as seen in Equation 2.33.

$$\begin{aligned} \begin{bmatrix} \dot{x}_1 \\ \dot{x}_2 \\ \dot{x}_3 \\ \dot{x}_e \end{bmatrix} &= \begin{bmatrix} -(k_{10}+k_{12}+k_{13}) & k_{21} & k_{31} & 0 \\ k_{12} & -k_{21} & 0 & 0 \\ k_{13} & 0 & -k_{31} & 0 \\ k_{1e} & 0 & 0 & -k_{e0} \end{bmatrix} \begin{bmatrix} x_1 \\ x_2 \\ x_3 \\ x_e \end{bmatrix} \\ &+ \begin{bmatrix} \frac{1}{V_1} \\ 0 \\ 0 \\ 0 \end{bmatrix} u(t-\tau_b) \qquad \cdot y = \begin{bmatrix} 0 & 0 & 0 & 1 \end{bmatrix} \begin{bmatrix} x_1(t-\tau_m) \\ x_2(t-\tau_m) \\ x_3(t-\tau_m) \\ x_e(t-\tau_m) \end{bmatrix} \end{aligned} \tag{2.33}$$

The non-delayed output states have the same delay value as the delayed state as seen in Equation 2.33. The matrix multiplication results in zero for non-delayed states. Therefore, it can be stated that these non-delayed states have no effect on the output of the model given in Equation 2.33.

The validity of the delayed model can be proven using patient data from VitalDB. The linear model system identification using the ARX model and hill curve approximation methods for surgical patient data from VitalDB have been presented in the previous subsection with correlation results. A similar method can be repeated for delayed model validation.

The method of validating the delayed patient model is to find the delay value that produces the highest correlation coefficient for each patient. System identifications for the Delayed ARX model (DARX) with sample delay values between 0 and 30 have been conducted for all 11 patients, and the delay values producing the highest correlation coefficient have been obtained for both CE and BIS data.

The parametric discrete-time transfer function model for 1 second of sampling time of the linear patient model with a delay of d samples can be written as seen in Equation 2.34. The DARX model derived from the parametric discrete-time transfer function is as seen in Equation 2.35, [70].

$$G_d(z) = \frac{\left(n_3 \cdot z^3 + n_2 \cdot z^2 + n_1 \cdot z^1 + n_0 \cdot z^0\right)}{\left(z^4 + d_3 \cdot z^3 + d_2 \cdot z^2 + d_1 \cdot z^1 + d_0 \cdot z^0\right)} \cdot z^{-d} \tag{2.34}$$

$$\begin{aligned} A\left(q^{-1}\right) y(k) &= B\left(q^{-1}\right) \cdot q^{-(d_t)} u(k) + e(k) \\ A\left(q^{-1}\right) &= \left(1 + d_3 \cdot q^1 + d_2 q^2 + d_1 q^3 + d_0 q^4\right) \\ B\left(q^{-1}\right) &= \left(n_3 q^{-(1+d_t)} + n_2 q^{-(2+d_t)} + n_1 q^{-(3+d_t)} + n_0 q^{-(4+d_t)}\right) \end{aligned} \tag{2.35}$$

The regression and parameter vectors of the linear regression seen in Equation 2.25 can be rewritten as seen in Equation 2.37 for the output delay case.

$$\varphi = \begin{bmatrix} -y(k-1) \\ -y(k-2) \\ -y(k-3) \\ -y(k-4) \\ u(k-1-d_t) \\ u(k-2-d_t) \\ u(k-3-d_t) \\ u(k-4-d_t) \end{bmatrix} \quad \hat{\theta} = \begin{bmatrix} -d_3' \\ -d_2' \\ -d_1' \\ -d_0' \\ n_3' \\ n_2' \\ n_1' \\ n_0' \end{bmatrix} \tag{2.36}$$

The system identification and linear regression for Hill curve approximation were run for all 11 patients for sample delay values that ranged between 0 and 30. The delay values that produce the highest correlation coefficient for each patient from CE data are as seen in Table 2.3

Table 2.3 : The delay values that produce the highest correlation coefficient from CE data.

Patient	delay [sample]	Correlation Coefficient
1	13.0000	0.9067
2	1.0000	0.9036
3	8.0000	0.8560
4	1.0000	0.9224
5	16.0000	0.9097
6	14.0000	0.9395
7	13.0000	0.7986
8	7.0000	0.9063
9	2.0000	0.9392
10	15.0000	0.9196
11	11.0000	0.9141

The delay values in Table 2.3 can be considered as biophase delays where the delay occurs in the output of the 4-compartmental linear patient model. The delay values that produce the highest correlation coefficient from BIS data are as seen in Table 2.4.

Table 2.4 : The delay values that produce the highest correlation coefficient from BIS data.

Patient	delay [sample]	Correlation Coefficient
1	18.0000	0.8917
2	25.0000	0.9684
3	20.0000	0.7532
4	12.0000	0.7386
5	19.0000	0.6529
6	24.0000	0.9388
7	17.0000	0.8365
8	15.0000	0.9109
9	17.0000	0.9625
10	28.0000	0.6356
11	16.0000	0.5750

It is possible to state from Table 2.4 that the delay values have increased compared to the delay values, which represents the biophase delays, given in Table 2.3. The

difference is caused by the monitor delay of the BIS monitor, which mostly ranges between 5 to 10 seconds, which corresponds to 5 to 10 samples while sampling time equals 1 second. The biophase delay and the monitor delay create the total output delay of the final delayed model given in Equation 2.37.

$$\begin{aligned} \dot{x}(t) &= A_p \cdot x(t) + B_p \cdot u(t - \tau_b) \\ y(t) &= k_h \cdot C_p \cdot x(t - \tau_m) + d_h \end{aligned} \tag{2.37}$$

The correlation analysis results with the final total delay values are as seen in Figure 2.15 where each bar in the graph represents the correlation coefficient for that patient between real data and final model outputs. The results and comparison of BIS values for the final delayed model output of all 11 patients are as seen in Figure A.3 in the Appendix.

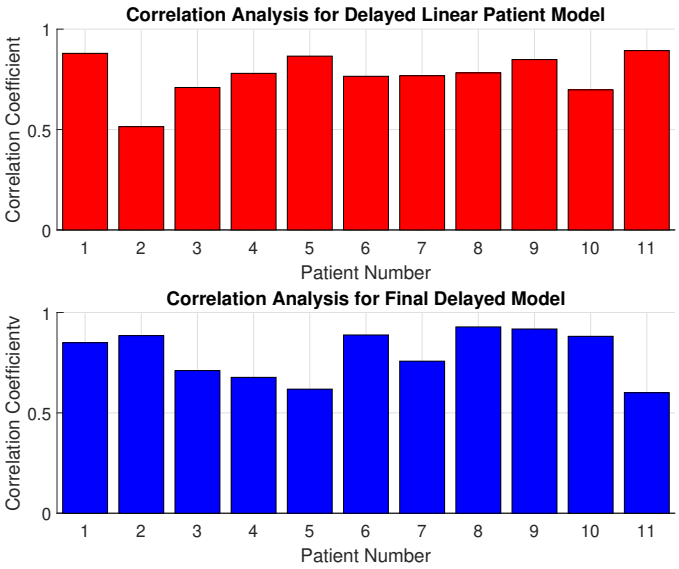

Figure 2.15 : The correlation analysis of final delayed model.

The mean value of the correlation coefficient for the delayed linear patient model with CE output equals 0.822, and the mean value of the correlation coefficient for the final delayed model with BIS output equals 0.807. The correlations of the final delayed model show a noticeable increase in terms of the mean values, while CE output shows a slight decrease. However, the mean values of both output correlations can be classified as strong correlations thanks to the modeling improvements using delays. Therefore,

the delayed models can be considered as valid according to the results. The extended models with output delays can be used in control applications.

The delayed models can be considered as 2 separate models Propofol input-CE output model with biophase delay and Propofol input-BIS output final delay models. In this situation, the delays take values from Tables 2.2 and 2.3. In such a case, it is possible to compare the correlation coefficients of these models with the correlation coefficients of patient models without delays depicted in Figure 2.14. The comparison of correlation coefficients is seen in Figure 2.16.

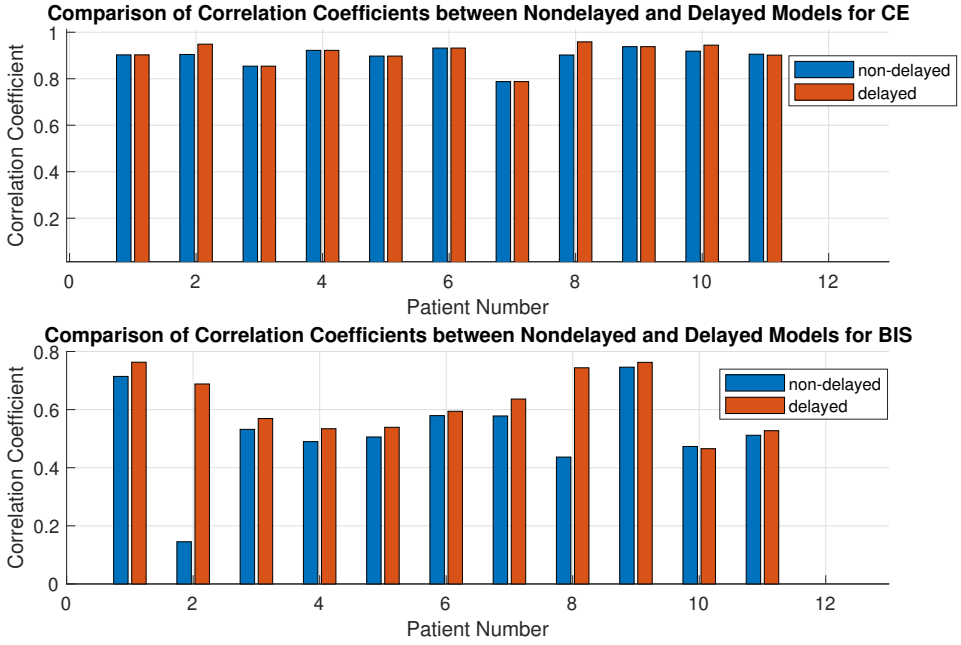

Figure 2.16 : Comparison of correlation coefficients between non-delayed and delayed models.

The correlation coefficients for final delayed models with BIS output are higher than the non-delayed models for nearly all patients with mostly large margins, according to Figure 2.16. Correlation coefficients of final delayed and non-delayed models with CE output also show that a similar statement is valid for CE cases with smaller margins.

In conclusion, the results show that PKPD patient models with output delays produce higher correlations with real patient data obtained from VitalDB, especially when the output is BIS. This situation is also important when the system's measurable output is BIS. According to the results, the delayed models can be considered valid. The extended models with output delays can be used in control applications.

3. INTER-PATIENT CONTROL OF ANESTHESIA

This chapter explains the common control methods used to control the hypnotic states of TIVA. The CL-TIVA performance criteria have been explained, and the PID-TIVA, SFC-TIVA, and MPC-TIVA method structures have been developed for the patient models. The simulation results have been obtained for both the 24-person parameter database and identified patient models using VitalDB data, which are explained in detail in the previous section.

3.1 Performance Criterias and Limitations

CL-TIVA aims to control the patient's hypnotic state according to specific performance criteria. These performance criteria are important for control performance as well as for the health and safety of the patient. In addition to transient time criteria, the determined closed-loop performance should also be evaluated for disturbance suppression, robustness against parameter uncertainties, inter-patient applicability, and adaptability to intra-patient changes.

The main criteria of CL-TIVA is to control the BIS to be constant at the value of 50. The performance criteria and control aims may change between different phases. Achieving a BIS value of 50 as quickly as possible is the goal during the induction phase of CL-TIVA. The BIS needs to be settled in 3-5 minutes for all patients, the overshoot should be less than % 10 for all patients, and the steady-state error should be less than % 2 for all patients during the induction phase. Controlling the BIS value near 50 is the main goal during the maintenance phase. The controller should be able to compensate for disturbances, parametric uncertainties, and time-varying changes by keeping the BIS value in the max-min interval of 40-60 during the maintenance phase to prevent dangerous hypnotic consequences [2,34].

The CL-TIVA also has limitations that restrict the controller's performance. The most significant ones concern the control signal. The control signal has saturations in its

value. It cannot be higher than $6.67[mg/s]$ or lower than $0[mg/s]$ [71]. Thus, the reverse infusion of propofol is not possible.

All the controller simulations have been conducted in this section for 3000 seconds. The controllers have been tested with and without the disturbances, while the effect of blood loss is permanent. The effect of blood loss starts at 1000 seconds, and the blood volume decreases with a linear slope starting from $4.27[L]$ and ending at $3[L]$ at 2500 seconds. The disturbance profile is as depicted in Figure 2.6. The performances of the controllers have been evaluated with IAE, which is calculated as seen in Equation 3.1.

$$IAE = \int_0^\infty |r(t) - BIS(t)|dt \tag{3.1}$$

3.2 PID Control

It is possible to suggest two different structures for implementing the PID controller into the hypnotic state control of CL-TIVA. These structures differ from each other according to the usage of the inverse hill curve function given in 2.14. The first structure, depicted in Figure 3.1, uses and implements the inverse Hill function to the closed loop structure. This structure's main feedback source can be considered as the CE, and the control loop in this structure can be called CE-Feedback PID-TIVA. The second structure, depicted in Figure 3.2, does not use and implements the inverse Hill function to the closed loop structure. This structure's main feedback source can be considered as the BIS, and the control loop in this structure can be called BIS-Feedback PID-TIVA.

The actual reference signal of this system is $r_{C_e}(t)$ and the main feedback source is $C_e(t)$. These values are calculated with the inverses Hill functions from $r_{BIS}(t)$ and $BIS(t)$. The compensation of nonlinearity is achieved through the inverse Hill curve, presented in 2.14, in a method also known as the exact linearization technique [46]. The important disadvantages of this structure can be considered as the complexity of implementation caused by additional calculation steps and the necessity of patient parameters. The suitable patient model for controller design using this structure is the patient model given in 2.12.

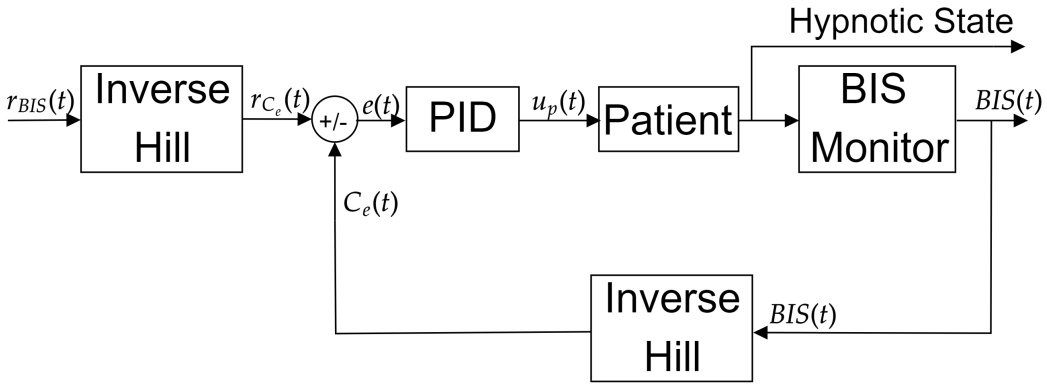

Figure 3.1 : CE-Feedback PID-TIVA structure.

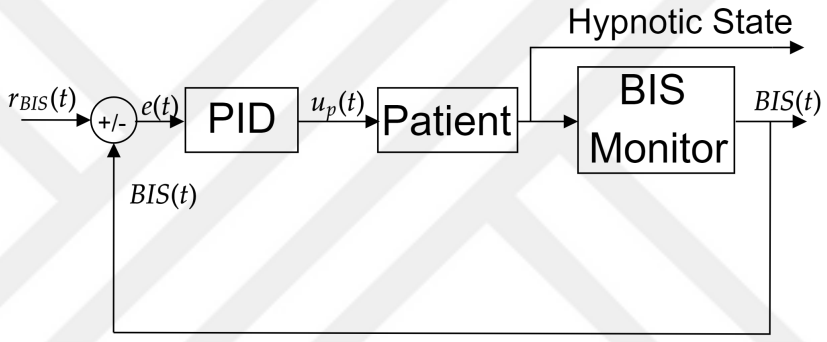

Figure 3.2 : BIS-Feedback PID-TIVA structure.

jmThe reference signal of this system is $r_{BIS}(t)$, and the main feedback source is $BIS(t)$ in this structure. The compensation of nonlinearity is achieved through the local linearization [46]. However, modeling errors and parametric uncertainties are expected to affect the CL-TIVA more than the exact linearization method in this model. The suitable patient model for controller design using this structure is the patient model given in 2.28.

PID controllers for both CE-Feedback PID-TIVA and BIS-Feedback PID-TIVA have been designed. The main goal of the PID-TIVA is to control the system without updating the model with patient parameters to increase inter-patient viability. Therefore, the PID controllers have been designed for the patient model with the nominal parameters in Table 2.1. The state space matrices of the nominal patient and

the pole-zero map are given in Equation 2.19 and Figure 2.9, respectively. The transfer function model of the nominal patient for CE output can be given as seen in Equation 3.2.

$$G_{p_{CE}}(s) = \frac{2.966 \cdot 10^{-5} s^2 + 3.66210^{-8} s + 2.042 \cdot 10^{-12}}{s^4 + 0.03186 s^3 + 0.0002669 s^2 + 2.13 \cdot 10^{-7} s + 8.119 \cdot 10^{-12}} \tag{3.2}$$

The first order shifted linear function obtained by the local linearization of the Hill curve for the nominal patient using LSE is as seen in Equation 3.3. The linear patient model for BIS output can be obtained as seen in Equation 3.4.

$$y(t) = -36.04 \cdot x(t) + 111.4 \tag{3.3}$$

$$G_{p_{BIS}}(s) = 111.4 - \frac{0.0008899 s^2 + 1.099 \cdot 10^{-6} s + 6.127 \cdot 10^{-11}}{s^4 + 0.03186 s^3 + 0.0002669 s^2 + 2.13 \cdot 10^{-7} s + 8.119 \cdot 10^{-12}} \tag{3.4}$$

The PID controllers have been designed using pole placement, and the desired dominant pole locations have been chosen as seen in Equation 3.5 while the desired settling time is 300 seconds and the desired overshoot is % 0.5.

$$\begin{aligned} s_1 &= -0.013333 + j0.060431 \\ s_2 &= -0.013333 - j0.060431 \end{aligned} \tag{3.5}$$

The PID controller structure used in PID-TIVA contains a back-calculation anti-windup mechanism to prevent the windup effect, which may increase the overshoot under inter-patient parametric uncertainty. The complete PID structure used in PID-TIVA is depicted in Figure 3.3. An additional K_b occurs for PID-TIVA with the back-calculation anti-windup mechanism. The PID parameters for CE-Feedback PID-TIVA and BIS-Feedback PID-TIVA structures, including back-calculation anti-windup parameters, have been obtained in Table 3.1.

The patient response signals as BIS output and the control signals of the nominal patient for CE-Feedback and BIS-Feedback PID-TIVA are as seen in Figure 3.4.

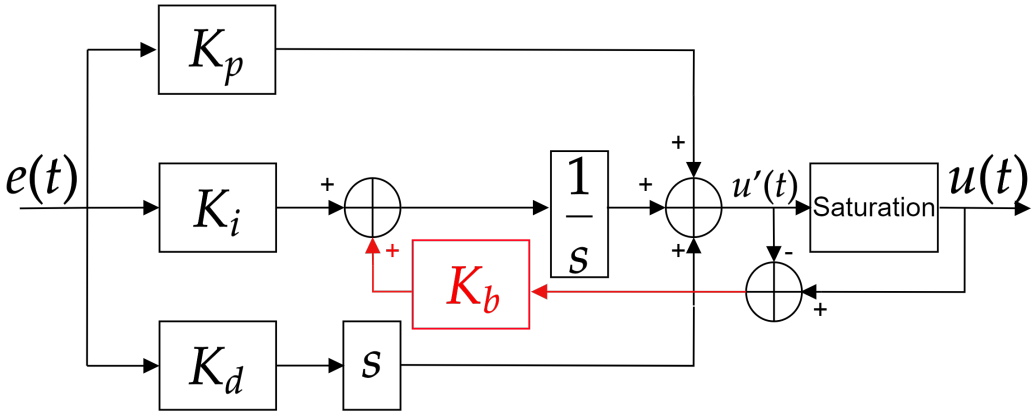

Figure 3.3 : The PID structure for PID-TIVA.

Table 3.1 : PID-TIVA Parameters

PID-TIVA	K_p	K_i	K_d	K_b
CE-Feedback	16.3	0.1452	473.8	0.01
BIS-Feedback	0.5432	0.004839	15.79	0.01

These responses are obtained under the effect of blood loss, without the effect of stimulation disturbances in order to obtain a better representation of the desired CL-TIVA performance.

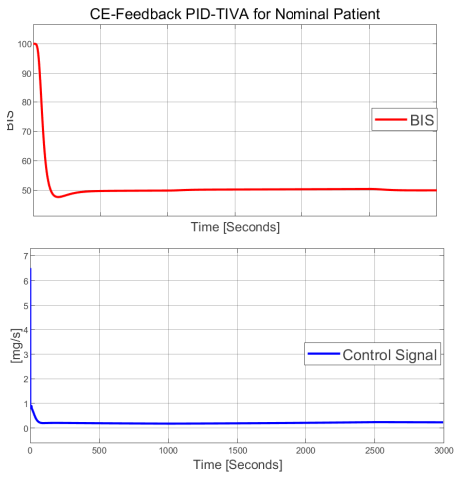

((a)) CE-Feedback PID-TIVA for the nominal patient.

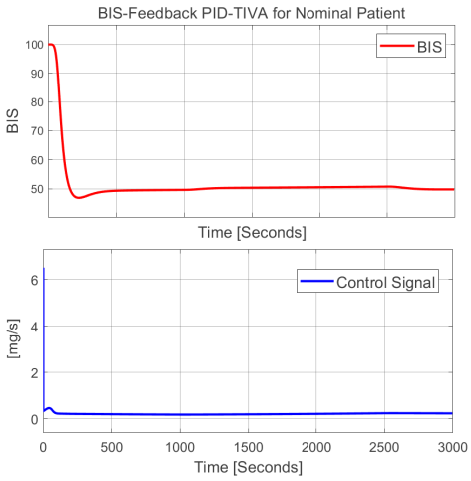

((b)) BIS-Feedback PID-TIVA for the nominal patient.

Figure 3.4 : CE-Feedback and BIS-Feedback PID-TIVA responses for the nominal patient.

The desired responses given in Figure 3.4 show that the transient response of the nominal patient model has been obtained as desired for both of the structures. The CE-Feedback PID TIVA structure shows a more robust performance than the BIS-Feedback PID TIVA structure when faced with changes in the patient's blood loss due to time-variant parametric uncertainty. This outcome is anticipated due to the improved patient model representation achieved through exact linearization utilizing the inverse hill curve, which is superior to local linearization using the first-order linear function.

The CL-TIVA responses using CE-Feedback and BIS-Feedback PID-TIVA controllers for the 24-patient database and VitalDB patients have been obtained for both cases while the stimuli disturbance is active and not. Figure 3.5 shows the responses without stimuli disturbances and figure 3.6 shows the responses with stimuli disturbances. The IAE values for CL-TIVA responses, calculated between the reference and system output, are in Table B.1 for each patient. The comparison of IAE values for each patient between PID-TIVA structures are as seen in Figure 3.7.

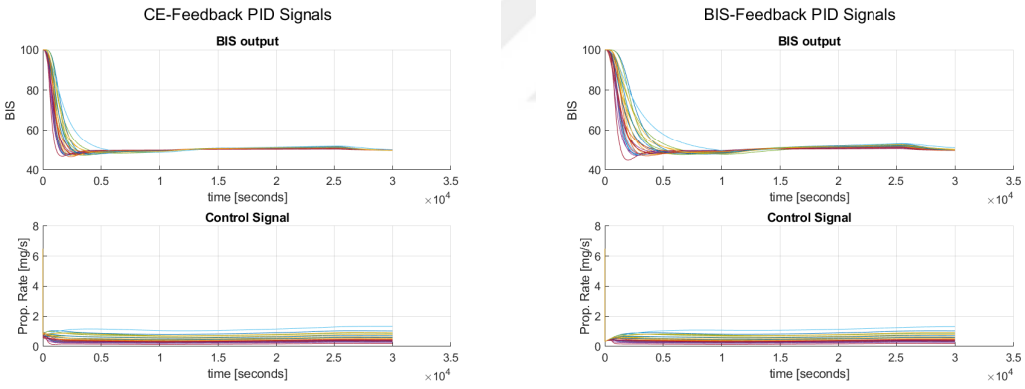

((a)) CE-Feedback PID signals.

((b)) BIS-Feedback PID signals.

Figure 3.5 : CE-Feedback and BIS-Feedback PID-TIVA responses for the 24-patient database without disturbance.

Figure 3.5 shows the transient responses and performances of the PID-TIVA controllers vary between different patients. It is possible to say that both of the PID-TIVA structures produce acceptable responses, which can defined as having a settling time below 380 seconds and an overshoot of less than %10 for the majority of the patients. However, several patients respond to PID-TIVA outside the acceptable area in both structures, which is more for the BIS-Feedback PID-TIVA structure. The

mean values of the IAE criteria for each structure without stimuli disturbances, 7048 for CE-Feedback PID-TIVA and 11364 for BIS-Feedback PID-TIVA, also support that suggestion.

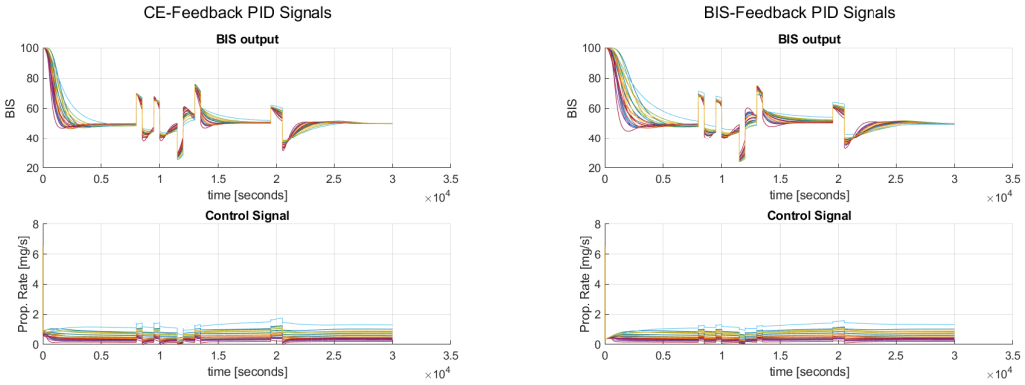

((a)) CE-Feedback PID signals. ((b)) BIS-Feedback PID signals.

Figure 3.6 : CE-Feedback and BIS-Feedback PID-TIVA responses for the 24-patient database with disturbance.

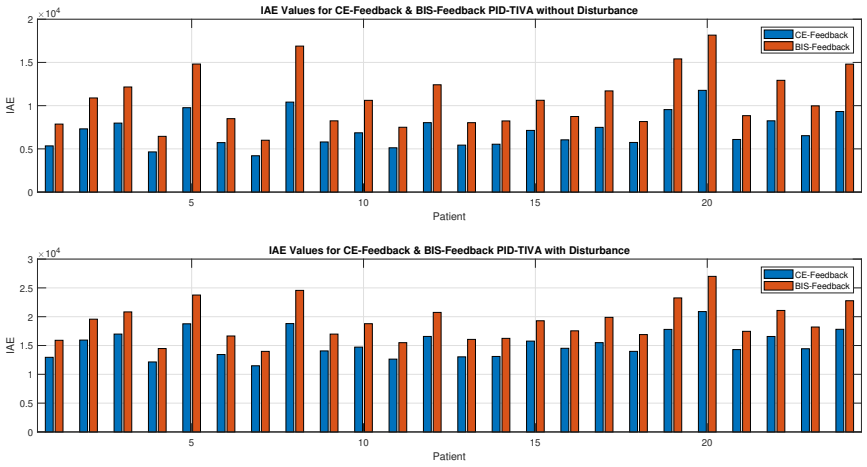

Figure 3.7 : Comparison of IAE values between PID-TIVA structures.

Figure 3.6 shows that the PID-TIVA controllers' disturbance compensation performances vary between patients. Several patients respond to PID-TIVA outside the acceptable area in both structures, which is more for the BIS-Feedback PID-TIVA structure as in case of stimuli disturbances. The mean values of the IAE criteria for each structure with stimuli disturbances, 15834 for CE-Feedback PID-TIVA and 19696 for BIS-Feedback PID-TIVA, also support that suggestion.

Overall, the CE-Feedback PID-TIVA structure performs more robust operations than the BIS-Feedback PID-TIVA structure for both the cases with and without stimuli disturbances. However, it is clear that the CE-Feedback PID-TIVA structure depends on the inverse hill curve parameters of the nominal patient parameters, which is nominal for a 24-patient database. That dependency may cause robustness issues with other patient groups and databases. Therefore, CE-Feedback and BIS-Feedback PID-TIVA structures have been tested with the patient models obtained using the VitalDB data for all 11 patients. Figure 3.8 shows the responses of 11 VitalDB patients for both CE-Feedback and BIS-Feedback PID-TIVA structures without stimuli disturbances and the effect of blood loss.

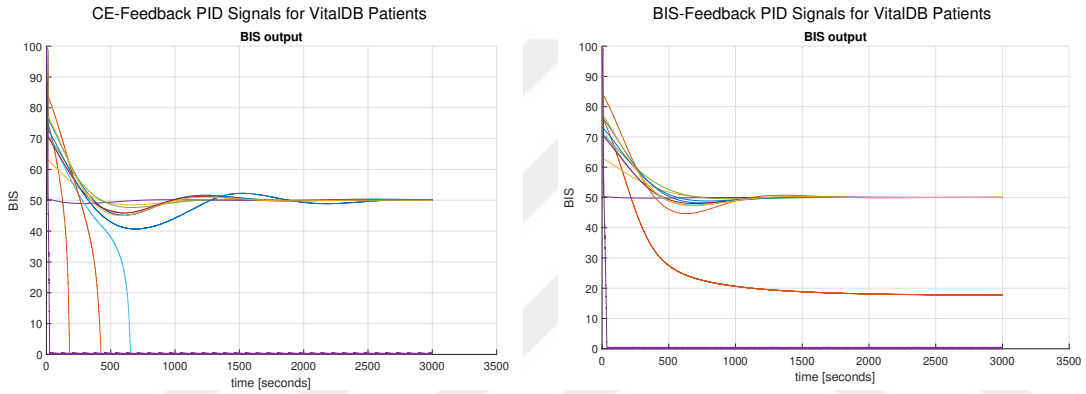

((a)) CE-Feedback PID signals for VitalDB patients.

((b)) BIS-Feedback PID signals for VitalDB patients.

Figure 3.8 : Responses of 11 VitalDB patients for PID-TIVA without disturbance.

Significant robustness issues have occurred for both of the PID-TIVA structures with VİtalDB patients. CE-Feedback could not assure CL-TIVA stability for 4 out of 11 patients, while this number is only 1 in BIS-Feedback PID-TIVA which is also unacceptable for a hypnotic state control system of TIVA. Moreover, the performance criteria were not met for all of the patients. Even though such issues occurred, BIS-Feedback PID-TIVA performed better inter-patient viability for models obtained from real patient surgical data and a larger patient database (combination of 24-patient DB and VitalDB) regarding stability. The PID-TIVA structures were also tested for VitalDB patients with stimuli disturbances. Figure 3.9 shows the responses of 11 VitalDB patients for both CE-Feedback and BIS-Feedback PID-TIVA structures without the effect of blood loss but with stimuli disturbances.

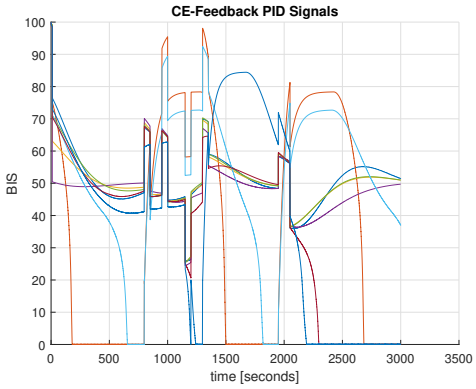

((a)) CE-Feedback PID signals for VitalDB patients.

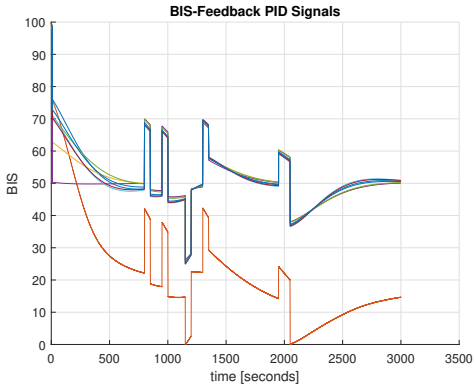

((b)) BIS-Feedback PID signals for VitalDB patients.

Figure 3.9 : Responses of 11 VitalDB patients for PID-TIVA with disturbance.

Figure 3.9 shows the disturbance has increased the stability issues for CE-Feedback PID-TIVA, while BIS-Feedback maintains the stability of all patients under disturbance. However, BIS-Feedback PID-TIVA's disturbance rejection performance is not satisfying due to the slow response under variant inter-patient parameters. The IAE values of CL-TIVA responses are in Table 3.3 for VitalDB patient.

Table 3.2 : IAE values of PID-TIVA for VitalDB patients

Patient	**Non-Disturbance**		**Disturbance**	
	CE-Feedback	**BIS-Feedback**	**CE-Feedback**	**BIS-Feedback**
Patient 1	7631.92	6860.00	19846.72	17490.68
Patient 2	144015.74	83769.32	104650.35	89751.80
Patient 3	3536.99	3990.46	14686.96	15419.17
Patient 4	1014.90	619.74	14200.63	11815.38
Patient 5	5442.94	6092.67	16707.97	17319.41
Patient 6	125334.05	5712.45	54489.03	16440.07
Patient 7	5909.00	5430.15	54135.55	16174.14
Patient 8	10994.38	6114.89	79462.44	16786.19
Patient 9	136349.80	9134.76	136349.80	9134.76
Patient 10	7242.63	7024.70	7242.63	7024.70
Patient 11	149356.34	149001.53	149356.34	149001.53
Mean	**44173.80**	**30369.15**	**47656.81**	**34767.89**

It is clear from the results given in Figure 3.8 and Figure 3.9 that BIS-Feedback PID-TIVA is more viable for inter-patient operations due to the nominal patient's inverse hill curve parameter dependency of CE-Feedback PID-TIVA structure. The mean IAE values of the BIS-Feedback PID-TIVA structure are lower than

CE-Feedback PID-TIVA for both cases. However, the performance criteria for both of the structures were not met. Therefore, a control structure to increase the inter-patient viability is required to be able to control both the 24-patient database and VitalDB patients as desired.

3.3 Lyapunov-Based MRAS Design

The adaptive control strategies can enhance the performance of control systems in situations where uncertainty is caused by factors like degradation and modeling uncertainty [72]. Regarding this, MRAS offers improved performance and robustness for inter-patient and intra-patient control of TIVA compared to PID-TIVA structures. The general MRAS structure for TIVA using the Reference Model and the Adaptation Law is depicted in Figure 3.10. $r_{BIS}(t)$ represents the reference input, which is also applied to the Reference Model, $y_{model}(t)$ is the output of the reference model system, $u_{prop}(t)$ is the control signal and $y_{BIS}(t)$ is the BIS output of the patient.

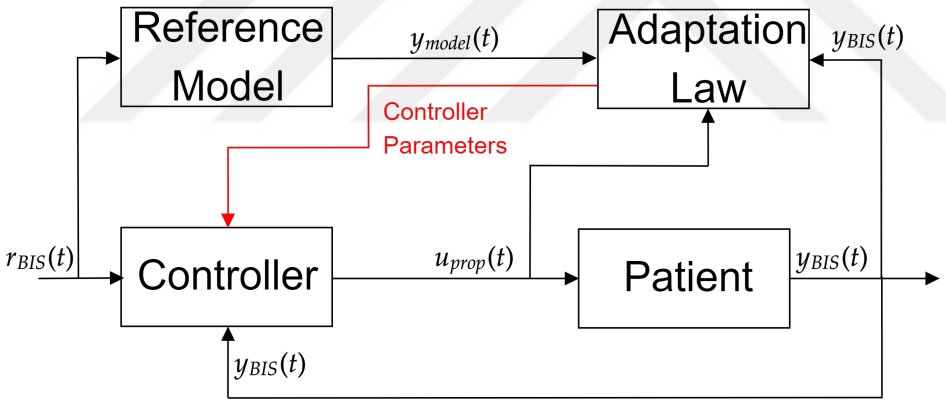

Figure 3.10 : The MRAS structure for TIVA.

The MRAS structure aims to control the TIVA under the intra-patient time-variant parameters caused by blood loss and under the inter-patient parametric uncertainties with the least nominal patient dependency. Therefore, the MRAS structure for TIVA uses the local linearization technique and considers the BIS value of the system's feedback source to increase inter-patient viability. The controller of the MRAS is an observer-based state feedback controller, and the adaptation law is based on Lyapunov's stability theorem. The MRAS-TIVA adapts the state feedback control

gains according to the adaptation law that is generated according to Lyapunov's stability theory. The MRAS structure can be investigated in detail as the reference model, observer-based state feedback controller, Lyapunov's theory-based adaptation law, implementation into TIVA, and database results in order. d

3.3.1 Observer Based State Feedback Control

State feedback control forms the basis of the MRAS-TIVA due to its availability to control and manipulate all the states of patient model. The control gains designed in observer-based state feedback control, K_{i_f} and M_i, are the initial gain values of MRAS-TIVA, which are getting adapted to compensate the error between the reference model and the system output according to the adaptation law generated by Lyapunov's stability theory. The control law of the state feedback control can be written as seen in Equation 3.6.

$$\begin{aligned} u(t) &= K_{i_f} \cdot u_c(t) - M_{i_1} \cdot x_1(t) - M_{i_2} \cdot x_2(t) - M_{i_3} \cdot x_3(t) - M_{i_4} \cdot x_4(t) \\ u(t) &= K_{i_f} \cdot u_c(t) - M_i \cdot x(t) \end{aligned} \tag{3.6}$$

K_f represents the feed-forward gain and the vector M represents the state feedback controller in Equation 3.6. The main problem with the state feedback controller is the inability to directly measure the states, which are defined as drug concentrations in blood, fat, and muscles. Therefore, a state observer is necessary to implement a state feedback controller for CL-TIVA. The diagram of state feedback control using a state observer is depicted in Figure 3.11. The control law can be updated as seen in Equation 3.7 using the state observer.

$$\begin{aligned} u(t) &= K_{i_f} \cdot u_c(t) - M_{i_1} \cdot x_{n_1}(t) - M_{i_2} \cdot x_{n_2}(t) - M_{i_3} \cdot x_{n_3}(t) - M_{i_4} \cdot x_{n_4}(t) \\ u(t) &= K_{i_f} \cdot u_c(t) - M_i \cdot x_n(t) \end{aligned} \tag{3.7}$$

3.3.1.1 State Feedback Controller Design

The design of the state feedback controller was conducted using the nominal patient parameters given in Table 2.1. The controllability matrix of the nominal patient model was calculated before the design of the state feedback controller, as seen in Equation 3.8.

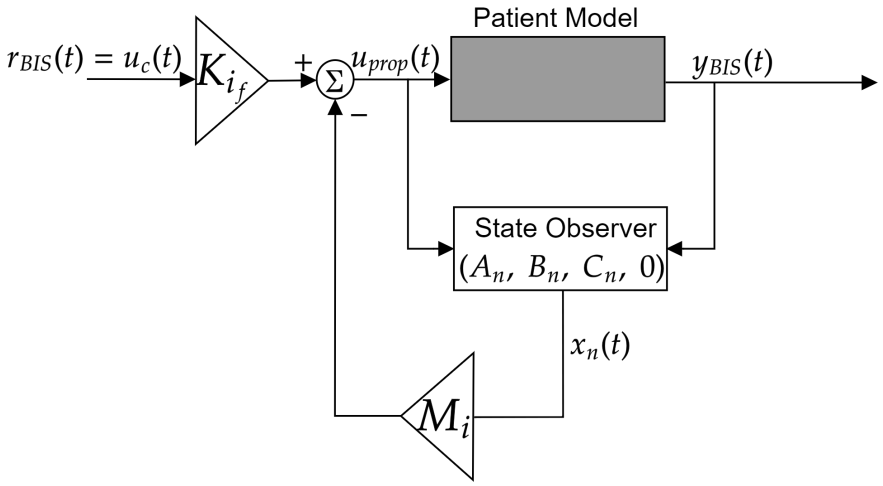

Figure 3.11 : The diagram of state feedback control using a state observer.

$$P = \begin{bmatrix} B_p & (A_p B_p) & (A_p{}^2 B_p) & (A_p{}^3 B_p) \end{bmatrix}$$
$$P = \begin{bmatrix} 0.0039 & -0.00005 & 0.0000008 & -0.00000001 \\ 0 & 0.00001 & -0.0000002 & 0.000000003 \\ 0 & 0.00001 & -0.0000001 & 0.000000002 \\ 0 & 0.00002 & -0.0000009 & 0.00000002 \end{bmatrix} \tag{3.8}$$

The rank of the controllability matrix equals 4, and the determinant of the matrix equals $6.0637 \cdot 10^{-24}$, which is nonzero. Even though the system can be considered controllable, the determinant of the controllability matrix is nearly zero. This situation may cause controllability issues under intra- and inter-patient operations of MRAS-TIVA. Therefore, the matrices have transformed into controllable canonical form using transformation matrices. It has been known that the controllable canonical for is always controllable. The transformation matrix and transformed model matrices can be calculated as seen in Equation 3.9.

$$\begin{aligned} T_{ccf} &= P \cdot P_{ccf}^{-1} \\ A_{ccf} &= T_{ccf}^{-1} \cdot A_p \cdot T_{ccf} \\ B_{ccf} &= T_{ccf}^{-1} \cdot B_p \\ C_{ccf} &= C_p \cdot T_{ccf} \end{aligned} \tag{3.9}$$

T_{ccf} represents the transformation matrix and A_{ccf}, B_{ccf}, C_{ccf} are the transformed forms of the model matrices. P_{ccf} can be calculated as seen in Equation 3.10.

$$P_{ccf} = \begin{bmatrix} B_{ccf} & (A_{ccf}B_{ccf}) & ({A_{ccf}}^2 B_{ccf}) & ({A_{ccf}}^3 B_{ccf}) \end{bmatrix} \tag{3.10}$$

The transformation matrix and model matrices in the controllable canonical form are as seen in Equations 3.11 and 3.12. "

$$T_{ccf} = \begin{bmatrix} 0.000000000004 & 0.00000007 & 0.00006 & 0.003 \\ 0.000000000014 & 0.0000002 & 0.00001 & 0 \\ 0.00000000024 & 0.0000002 & 0.00001 & 0 \\ 0.000000000002 & 0.00000003 & 0.00002 & 0 \end{bmatrix} \tag{3.11}$$

$$\begin{aligned} A_{ccf} &= \begin{bmatrix} 0 & 1 & 0 & 0 \\ 0 & 0 & 1 & 0 \\ 0 & 0 & 0 & 1 \\ -0.000000000008 & -0.0000002 & -0.0003 & -0.0319 \end{bmatrix} \\ B_{ccf} &= \begin{bmatrix} 0 \\ 0 \\ 1 \end{bmatrix} \\ C_{ccf} &= 10^{-4} \cdot \begin{bmatrix} 0.00000002 & 0.0004 & 0.2966 & 0 \end{bmatrix} \end{aligned} \tag{3.12}$$

The controller parameters have been calculated using Ackermann's pole placement method for the dominant pole positions given in Equation 3.13. The Ackermann's formula for pole placement is in Equation 3.14

$$\begin{aligned} \lambda_1 &= -0.26333 + j0.060431 \\ \lambda_2 &= -0.26333 - j0.060431 \\ \lambda_3 &= -0.0012 \\ \lambda_4 &= -0.000049 \end{aligned} \tag{3.13}$$

$$M = [0 \quad 0 \quad 0 \quad 1] \cdot {P_{ccf}}^{-1} \cdot \alpha(A_{ccf}) \tag{3.14}$$

The poles closer to the origin λ_3 and λ_4 have been used to compensate for the effect of zeros close to the origin depicted in Figures 2.8 and 2.9. λ_1 and λ_2 acts like the dominant poles in this situation. λ_1 and λ_2 have chosen 20 times farther in the left than the dominant poles given in Equation 3.5 in order to compensate the error faster, which are also the dominant poles of the reference model of MRAS-TIVA. The actual performance criteria of MRAS-TIVA are defined by the Reference Model.

$\alpha(A)$ is the desired polynomial as a function of the matrix A_{ccf}. The desired polynomial and $\alpha(A)$ are as seen in Equation 3.15

$$\alpha(s) = s^4 + 0.02795s^3 + 0.0002122s^2 + 2.307 \cdot 10^{-7}s + 1.091 \cdot 10^{-11}$$
$$\alpha(A_{ccf}) = {A_{ccf}}^4 + 0.02795{A_{ccf}}^3 + 0.0002122{A_{ccf}}^2 + 2.307 \cdot 10^{-7}A_{ccf} + 1.091 \cdot 10^{-11} \tag{3.15}$$

The feed-forward gain K_{i_f} has been calculated in Equation 3.14 to eliminate the steady-state error. The state feedback controller gains have been calculated as seen in Table 3.3.

$$K_{i_f} = \frac{1}{C_{ccf}(-A_{ccf} + B_{ccf}M_i)^{-1}B_{ccf}} \tag{3.16}$$

Table 3.3 : SFC-TIVA Parameters

	K_{i_f}	M_{i_1}	M_{i_2}	M_{i_3}	M_{i_4}
SFC	54.17	0.000000004	0.00009	0.07	0.499

3.3.1.2 Observer Design

The state feedback controller and MRAS-TIVA use a Kalman filter-based state observer. The Kalman filter provides the basic and precise recursive least squares algorithm for time-varying system parameters [73]. Therefore, the Kalman filter is suitable for intra-patient, caused by the effect of blood loss and inter-patient operations of CL-TIVA. The C-Time measurement and the C-Time Kalman filter equations for nominal patient model matrices in controllable canonical form are in Figures 3.17 and 3.18, respectively [74]. Here, $w_{syr}(t)$ and $v_{BIS}(t)$ are continuous-time white noise processes, which can be considered as the noise of the BIS monitor and syringe pumps. The state estimations of TIVA using Kalman Filter are also presented in [75].

$$\begin{aligned} \dot{x_n}(t) &= A_{ccf}x_n + B_{ccf}u_{prop} + w_{syr} \\ y_{BIS}(t) &= C_{ccf}x_n + v_{BIS} \\ w_{syr} &\sim (0, Q_c) \\ v_{BIS} &\sim (0, R_c) \end{aligned} \tag{3.17}$$

$$
\begin{aligned}
\hat{x_n}(0) &= E[x_n(0)] \\
P_k(0) &= E\left[(x_n(0)-\hat{x_n}(0))(x_n(0)-\hat{x_n}(0))^T\right] \\
K_{kalman} &= P_k C_{ccf}^T R_c^{-1} \\
\dot{\hat{x_n}} &= A_{ccf}\hat{x_n} + B_{ccf}u_{prop} + K_{kalman}(y_{BIS}(t) - C_{ccf}\hat{x_n}) \\
\dot{P_k} &= -P_k C_{ccf}^T R_c^{-1} C_{ccf} P_k + A_{ccf}P_k + P_k A_{ccf}^T + Q_c
\end{aligned}
\tag{3.18}
$$

The state feedback controller uses the state estimations $x_n(t)$ as seen in Figure 3.11.

3.3.2 Model Reference Adaptive Controller

The MRAC tunes SFC gain parameters as the error changes. The error corresponds to the difference between real patient signals and the reference model. Lyapunov's theory-based adaptation law adapts SFC gains to compensate for the error. The SFC gain parameters are the initial values of controller parameters. The actual control law of MRAC is given in Equation 3.19.

$$
\begin{aligned}
u(t) &= (K_{i_f} + K_L)\cdot u_c(t) - (M_i + M_L)\cdot x(t) \\
u(t) &= K_f \cdot u_c(t) - M \cdot x(t) \\
K_f &= (K_{i_f} + K_L) \\
M &= (M_i + M_L)
\end{aligned}
\tag{3.19}
$$

K_L and M_L represent the tuning values of SFC gains. K_f and M are the final-tuned values of the controller. The MRAC can be investigated in detail, such as the choice of reference model, Lyapunov's theory, and implementation of TIVA.

3.3.2.1 Reference Model

The choice of the reference model determines the actual performance criteria and desired outputs of MRAS-TIVA. The reference model of the MRAS-TIVA has been chosen according to the desired performance criteria as 300 seconds of settling time and %0.5 maximum overshoot. The dominant poles of the reference model are the same as the poles given in Equation 3.5.

The reference model is built in controllable canonical form. Therefore, the states of the reference model do not correspond to drug concentrations of compartments. However,

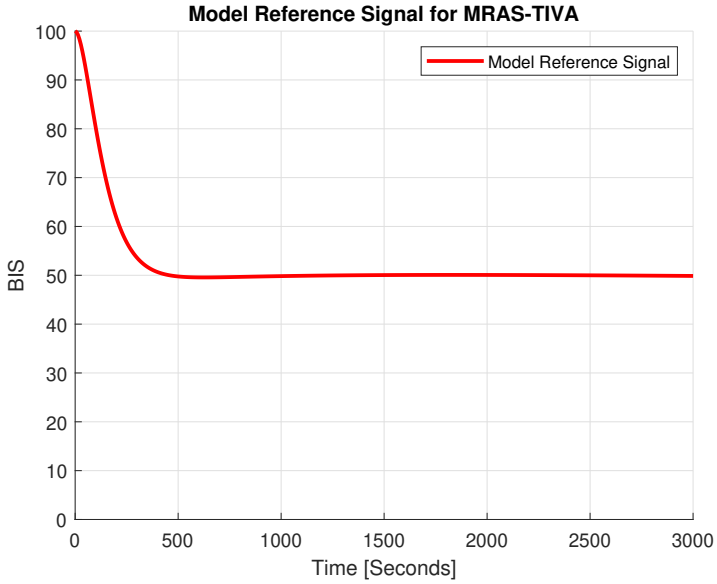

Figure 3.12 : Model reference signal for MRAS-TIVA.

compensation for the error that occurs on model states is required to control the system and make it converge into the reference model. The reason for the state observer given in Equation 3.18 to be in the controllable canonical form is to obtain the reference state signals in the same form. The error has been calculated as the difference between reference state signals and the reference signals of the patient model in controllable canonical form. The desired state signals are as given in Figure 3.13.

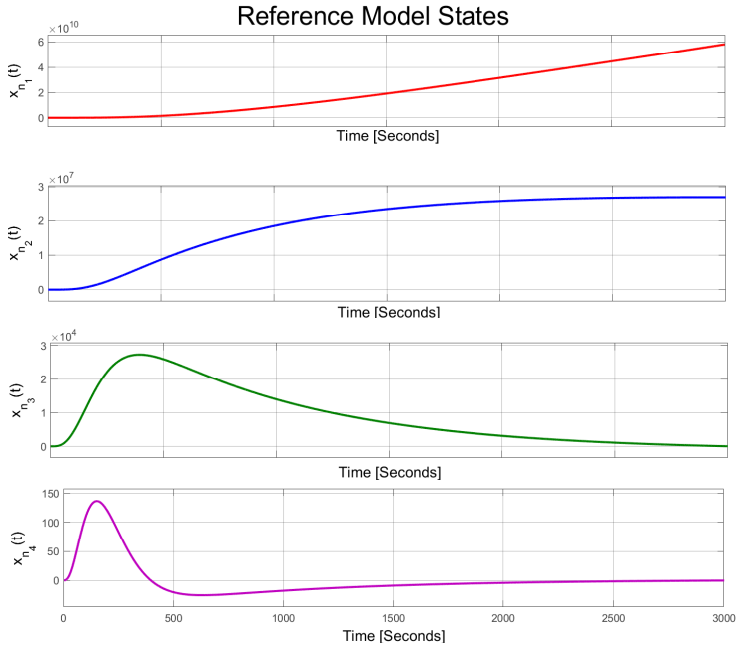

Figure 3.13 : States of the reference model.

3.3.2.2 Lyapunov's Theory and Adaptation Laws

The CCF patient and CCF reference models can be re-written in the forms given in Equations 3.20 and 3.21, respectively [76].

$$\frac{dx}{dt} = Ax + Bu \tag{3.20}$$

$$\frac{dx_m}{dt} = A_m x_m + B_m u_c \tag{3.21}$$

The matrix A and the vector B are the patient model matrices in CCF. The matrix A_m and the vector B_m are the reference model matrices in CCF. The final control law of MRAS-TIVA can be rewritten as in Equation 3.22.

$$u(t) = K_f \cdot u_c(t) - M \cdot x(t) \tag{3.22}$$

The error between reference state signals and the reference signals of the patient model can written as in Equation 3.23. Here, x is the states of the patient model, and x_m is the states of the reference model, both in CCF.

$$e = x - x_m \tag{3.23}$$

After declaring these definitions, the purpose of the MRAC's adaptation law can be determined as the convergence of the error to zero. A differential equation of the error expression can be produced by taking the derivative of the error. This differential equation defines a dynamic for the error function while making it t converge zero is aimed [76]. The derivative of error is in Equation 3.24.

$$\begin{aligned} \frac{de}{dt} &= \frac{dx}{dt} - \frac{dx_m}{dt} \\ \frac{de}{dt} &= Ax + Bu - A_m x_m - B_m u_c \end{aligned} \tag{3.24}$$

The dynamical equation of error can turn into a first-order differential equation with after steps such as adding and subtracting $A_m x$ from both left and right sides as seen in

Equation 3.25.

$$\begin{aligned} A_m x + \dot{e} &= Ax + Bu + A_m x - A_m x_m - B_m u_c \\ A_m x + \dot{e} &= Ax + Bu + A_m e - B_m u_c \\ \dot{e} &= -A_m x + Ax + Bu + A_m e - B_m u_c \\ \dot{e} &= A_m e + (A - A_m)x + Bu - B_m u_c \end{aligned} \tag{3.25}$$

The $\dot{e}$ can be re-written in closed loop form by adding the control law given in Equation 3.22 to $\dot{e}$ through u as given in Equation 3.26.

$$\begin{aligned} \dot{e} &= A_m e + (A - A_m)x + B(K_f \cdot u_c - M \cdot x) - B_m u_c \\ \dot{e} &= A_m e + (A - A_m - BM)x + (BK_f - B_m)u_c \end{aligned} \tag{3.26}$$

The Lyapunov function candidate can be suggested for adjusting M and K_f parameters to their proper values, as seen in Equation 3.27, where $A - BM - A_m = A(M)$ and $BK_f - B_m = B(K_f)$. Here $\Gamma = [\gamma_2 \quad \gamma_3 \quad \gamma_4 \quad \gamma_5]^T$. $\gamma_1, \Gamma \text{and} \gamma_6$ represent the free-parameters of MRAC design.

$$V(e, K_f, M) = \frac{1}{2}\left(\gamma_1 e^T P e + \Gamma(A(M)^T P(A(M)) + \gamma_6 (B(K_f))^T (B(K_f))\right) \tag{3.27}$$

The Lyapunov function candidate should obey the following rules to be defined as the Lyapunov function for time-variant systems: [76].

- $V(0) = 0$
- $V(x,t)$ should be positive-definite
- $V(x,t)$ should be bounded by a non-time dependent function, such as being bounded to e, to prove the stability of the time-variant system.
- $\frac{dV}{dt}$ should be negative-semi definite [76].

The Lyapunov function candidate $V(e, K_f, M)$ is positive definite while P is a positive-definite matrix and also depends on e. $\frac{dV}{dt}$ can written as in Equation 3.28 for investigation of being negative-semi definite. Here Q is a positive definite matrix calculated as seen in Equation 3.29.

$$\frac{dV}{dt} = -\frac{\gamma_1}{2} e^{\tau} Q e + \Gamma\left(A(M)\right) x^T P e + \left(A(M)\right)^T \frac{dM}{dt} + B(K_f)\left(\frac{dK_f}{dt} + \gamma_6 u_c B^T P x\right)$$

$$\frac{dV}{dt} = -\frac{\gamma_1}{2} e^{\tau} Q e + A(M)^T \left(\frac{dM}{dt} + \Gamma x^T P e\right) + B(K_f)\left(\frac{dK_f}{dt} + \gamma_6 u_c B^T P x\right) \tag{3.28}$$

$$A_m^T P + P A_m = -Q \tag{3.29}$$

The adaptation law can be chosen for eliminating the $A(M)$ and $B(K)$ terms according to [76] as seen in Equation 3.30.

$$\begin{aligned} \frac{dM}{dt} &= -\Gamma x^T P e \\ \frac{dK_f}{dt} &= -\gamma_6 u_c B^T P x \end{aligned} \tag{3.30}$$

The statement in Equation 3.31 can be done according to Kalman-Yakubovich Lemma if the system is controllable and observable [77] where P is a positive-definite matrix.

$$\begin{aligned} B^T P &= C \\ B^T P x &= C x = e \end{aligned} \tag{3.31}$$

Overall, the adaptation laws can be written as seen in Equation 2.37 when Γ and γ_6 are substituted with α and β, respectively.

$$\begin{aligned} \frac{dM}{dt} &= -\alpha x^T P e \\ \frac{dK_f}{dt} &= -\beta u_c e \end{aligned} \tag{3.32}$$

3.3.2.3 Implementation and Results of MRAS-TIVA

The adaptation laws given in Equation 3.32 can be implemented to TIVA as seen in Equations 3.33 and 3.34. The final values of controller gains are as seen in Equation 3.35.

$$\frac{dM_L}{dt} = -\begin{bmatrix} \alpha_1 \\ \alpha_2 \\ \alpha_3 \\ \alpha_4 \end{bmatrix} \cdot \begin{bmatrix} x_{n_1} & x_{n_2} & x_{n_3} & x_{n_4} \end{bmatrix} \cdot P \cdot \begin{bmatrix} x_{n_1} - x_{m_1} \\ x_{n_2} - x_{m_2} \\ x_{n_3} - x_{m_3} \\ x_{n_4} - x_{m_4} \end{bmatrix} \tag{3.33}$$

$$\frac{dK_L}{dt} = -\beta u_c \left(x_n - C_m \cdot x_m\right) \tag{3.34}$$

$$\begin{aligned} K_f &= (K_{i_f} + K_L) \\ M &= (M_i + M_L) \end{aligned} \tag{3.35}$$

The free parameters of MRAC design defined as α and β have been selected as given in Equation 3.36.

$$\alpha = \begin{bmatrix} \alpha_1 \\ \alpha_2 \\ \alpha_3 \\ \alpha_4 \end{bmatrix} = \begin{bmatrix} 10^{-17} \\ 10^{-13} \\ 10^{-7} \\ 10^{-15} \end{bmatrix} \tag{3.36}$$

$$\beta = -0.00135$$

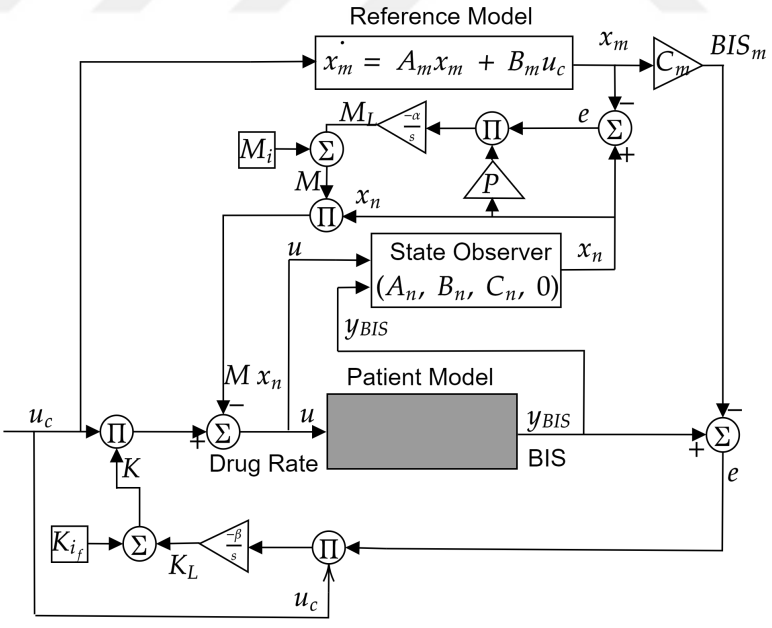

Figure 3.14 : The diagram of state feedback control using a state observer.

The diagram of implementing the state-observer bases state feedback controller and adaptation rules to MRAS-TIVA is as depicted in Figure 3.15. The MRAS given in

Figure 3.14 has been applied to both 24-patient and VitalDB databases to evaluate MRAS-TIVA in intra- and inter-patient viability. The results have been obtained in cases with disturbance and non-disturbance. The results for 24 patients without stimuli disturbance are as seen in Figure 3.15 while the effect is blood loss is persistent. The results for 24 patients with stimuli disturbance are as seen in Figure 3.18 while the effect is blood loss is persistent. The IAE values of both cases are given in Table C.1.

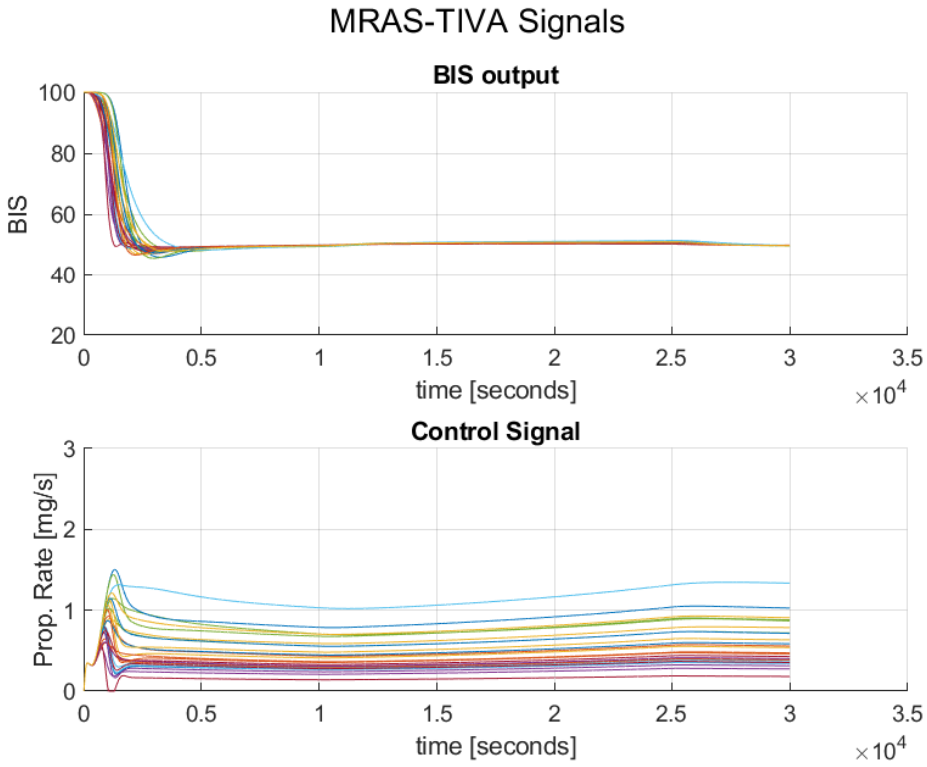

Figure 3.15 : MRAS-TIVA signals for 24 patient DB without stimuli disturbance.

Figure 3.15 shows that the transient responses and performances of MRAS-TIVA are acceptable. All the patients settled to the BIS value of 50 near the desired settling times, and the overshoots of all patients are below %10. The effect of blood loss, which starts at the second 1000, is compensated for all patients as the control signals increase after the second 1000. The mean value of IAE values for the case without stimuli disturbances, given in Table C.1, have been obtained as $7918,17$. The adjustment of control gains K and M by the adaptation laws, given in Equations 3.33 and 3.34, is as depicted in Figures 3.16 and 3.17, respectively.

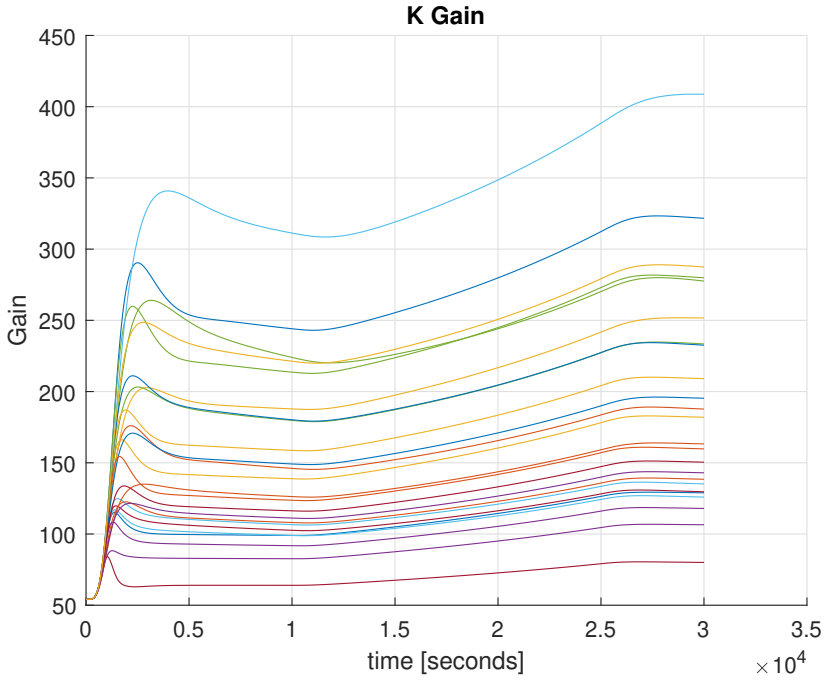

Figure 3.16 : Adjustment of the feed-forward gain K.

Figure 3.16 shows the adjustment of the feed-forward gain K during the MRAS-TIVA for 24-patient DB. It is possible to say that the K gain has been adapted by the adaptation laws for each patient to provide inter-patient feasibility. Moreover, the K gain has been adapted against the effect of blood loss as the increase after the second 1000 shows for each patient, which ensures intra-patient feasibility.

Figure 3.17 shows the adjustment of the state feedback controller gains M during the MRAS-TIVA for 24-patient DB. It is possible to say that the M gain has been adapted by the adaptation laws for each patient to provide inter-patient feasibility, even though the change in parameters was minor when it is compared with K. Moreover, it is possible to say that the effect of blood loss has mostly been compensated by the adjustment of K.

Figure 3.18 shows that MRAS-TIVA was able to compensate for the stimuli disturbance and maintain the hypnotic state of all 24 patients under both stimuli disturbances and the effect of blood loss. Control signals of MRAS-TIVA under stimuli disturbances show that the controller has reacted to stimuli and blood loss. The mean value of IAE values for the case without stimuli disturbances, given in Table C.1, have been obtained as $14824,79$.

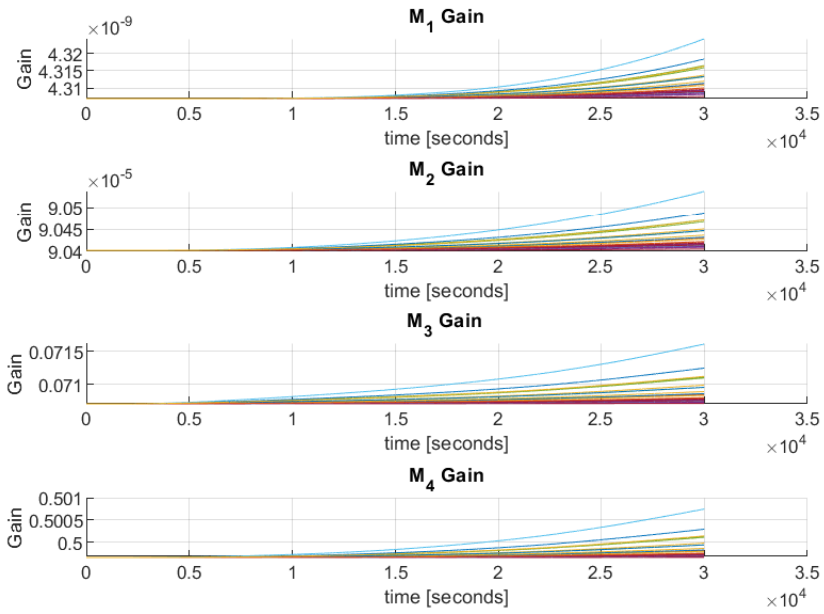

Figure 3.17 : Adjustment of the state feedback controller gains M.

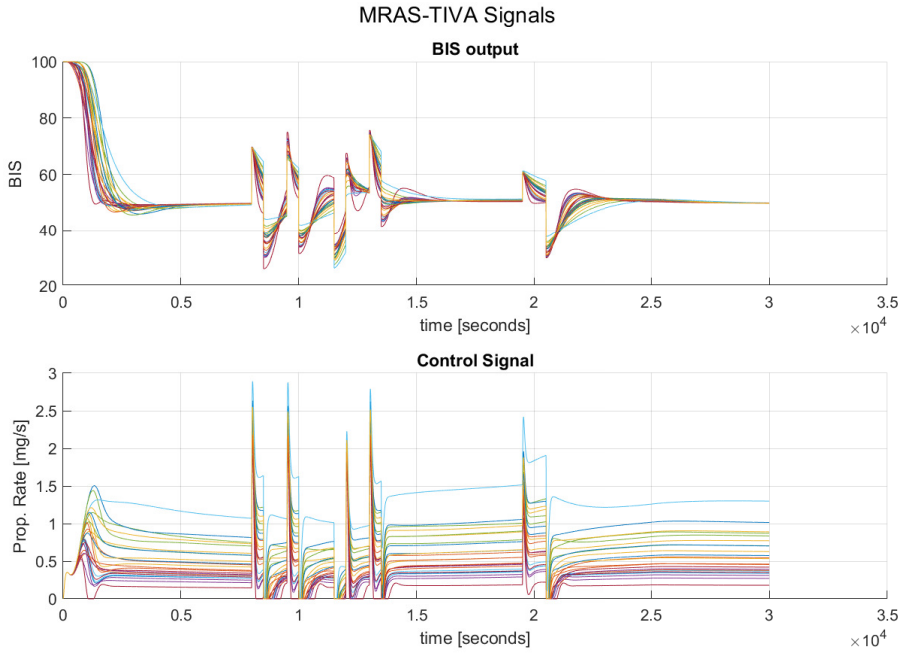

Figure 3.18 : MRAS-TIVA signals for 24 patient DB with stimuli disturbance.

The MRAS-TIVA was tested using VitalDB surgical data with 11 patient models to evaluate its robustness performance in cases with and without stimuli disturbances while ignoring the effect of blood loss. MRAS-TIVA signals for VitalDB patients

without stimuli disturbances are as seen in Figure 3.19 and with stimuli disturbances are as seen in Figure 3.20.

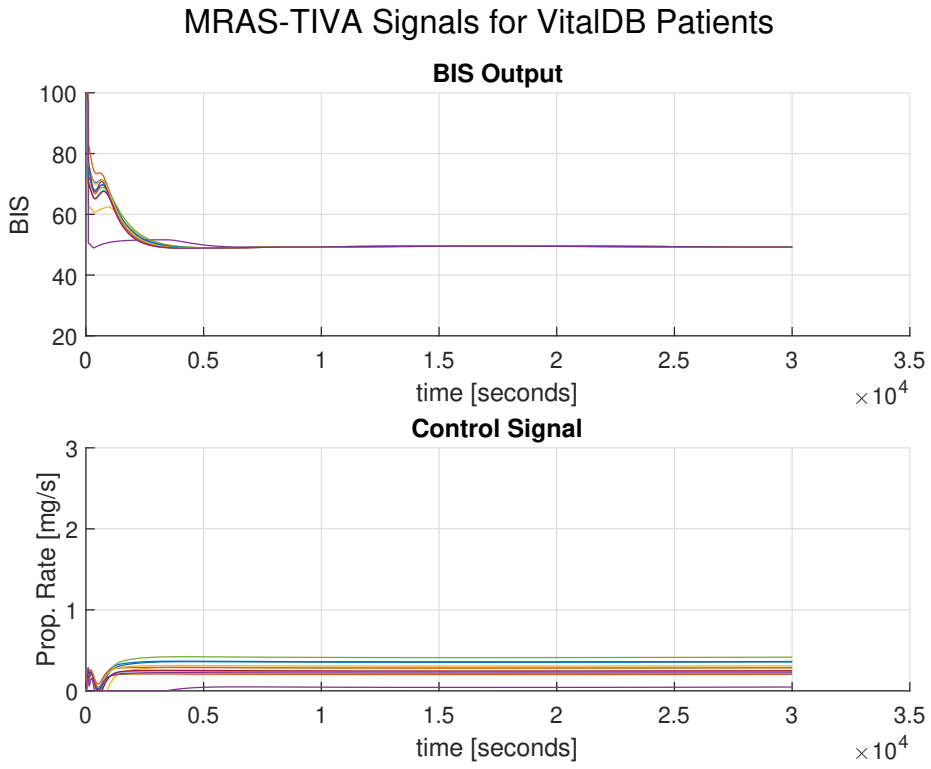

Figure 3.19 : MRAS-TIVA signals for VitalDB patients without stimuli disturbances.

Figure 3.19 shows that the MRAS-TIVA was able to control all 11 patients of the VitalDB patient models. In addition to preserving their stability, transient time responses were also achieved at the desired levels. Moreover, the control signal levels are lower than those of the 24-patient DB control signals. The adjustments of control gains K and M by the adaptation laws are as seen in Figures 3.20 and 3.21, respectively.

Figure 3.20 shows the adjustment of the feed-forward gain K during the MRAS-TIVA for VitalDB patients. It is possible to say that the K gain has been adapted by the adaptation laws for each patient to provide inter-patient feasibility. One of the K values has taken negative values, but the stability of the system is maintained.

Figure 3.21 shows the adjustment of the state feedback controller gains M during the MRAS-TIVA forVitalDB patients. It is possible to say that the M gain has been adapted by the adaptation laws for each patient to provide inter-patient feasibility, even though the change in parameters was minor when it is compared with K.

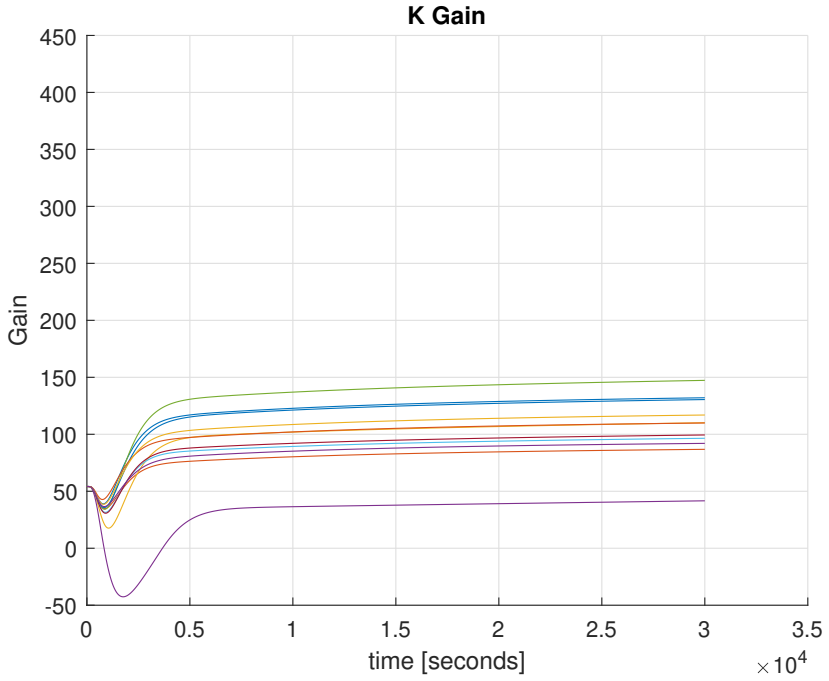

Figure 3.20 : Adjustment of the feed-forward gain *K* for VitalDB patients.

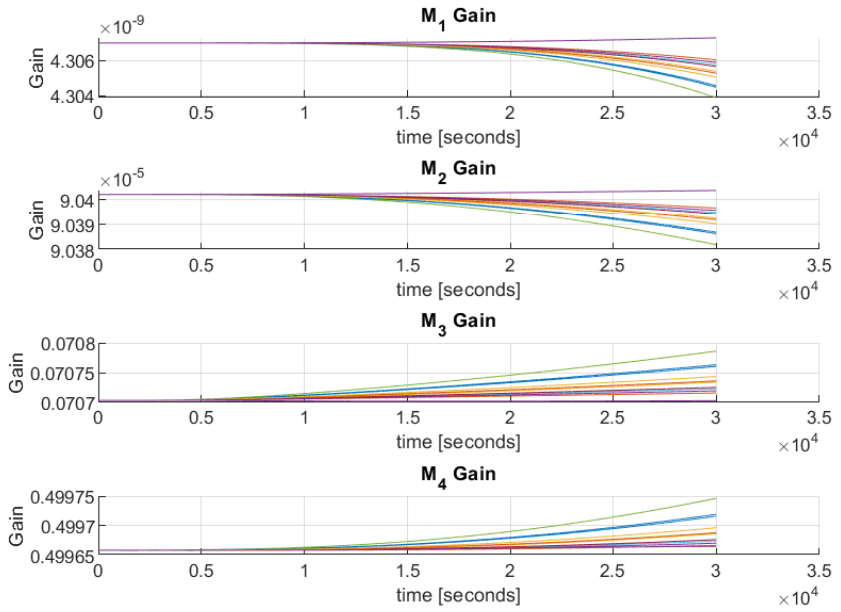

Figure 3.21 : Adjustment of the feed-forward gain *M* for VitalDB patients.

The results of MRAS-TIVA on VitalDB patients have also been obtained for the case with stimuli disturbances, as seen in Figure 3.22.

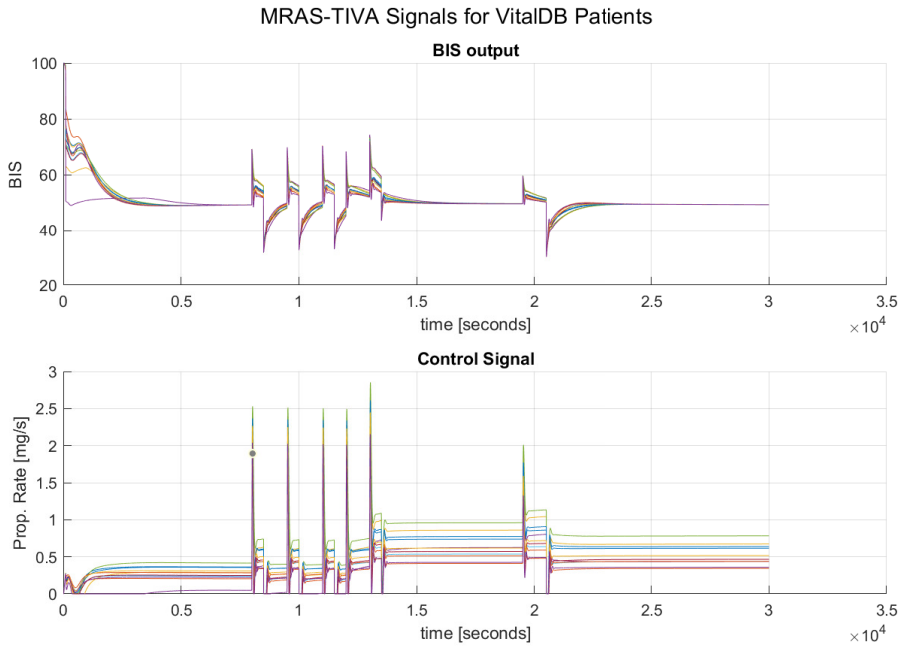

Figure 3.22 : MRAS-TIVA signals for VitalDB patients with stimuli disturbances.

Figure 3.22 shows that the MRAS-TIVA was able to control all 11 patients of the VitalDB patient models under stimuli disturbances without any issues with stability and transient response criteria. The MRAC reacted against the stimuli and compensated the disturbance for all patients. The IAE values of VitalDB patients with and without stimuli disturbances are as seen in Table 3.4.

Table 3.4 : The IAE values of VitalDB patients

Patient	Non-disturbance	Disturbance
Patient 1	5364.6	8574.1
Patient 2	4968.6	7424.8
Patient 3	4477.0	9090.1
Patient 4	2668.5	7819.3
Patient 5	5251.1	9512.9
Patient 6	4893.4	8047.2
Patient 7	4871.3	8141.4
Patient 8	5166.1	8499.4
Patient 9	5493.0	7903.7
Patient 10	5267.1	8083.0
Patient 11	5024.4	7070.8
Mean	**4820.64**	**8181.5**

The results obtained from MRAS-TIVA show that the designed MRAC has been able to settle the hypnotic state near the desired transient responses during the infusion state and maintain the desired hypnotic state under stimuli disturbances and the effect of blood loss for 3000 seconds. The MRAS-TIVA has proved its feasibility for intra- and inter-patient operations for both 24-patient DB and VitalDB patients.

3.4 Comparisons

The results of MRAS-TIVA can compared with BIS-Feedback PID-TIVA results for 24-patient DB and VitalDB patients due to the inter-patient validity of these methods both on the 24-patient database and VitalDB patients. The comparison of IAE values for both the cases on 24-patient DB with and without stimuli disturbances is seen in Figure 3.23.

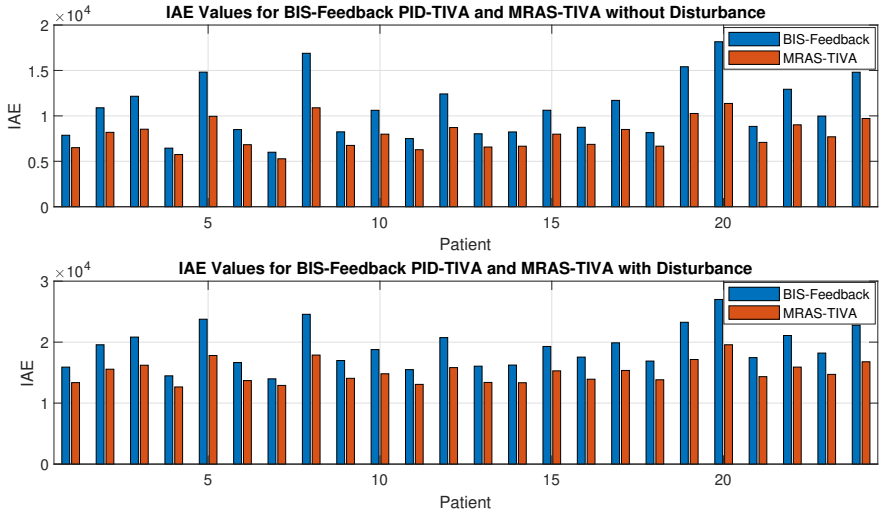

Figure 3.23 : Comparison of IAE values between BIS-Feedback PID-TIVA and MRAS-TIVA.

It is possible to say from Figure 3.23 that the IAE values of BIS-Feedback PID-TIVA are higher than MRAS-TIVA for all patients in both cases. This result supports the suitability of MRAS-TIVA. The comparison of IAE values on VitalDB patients with and without stimuli disturbances is seen in Figure 3.23.

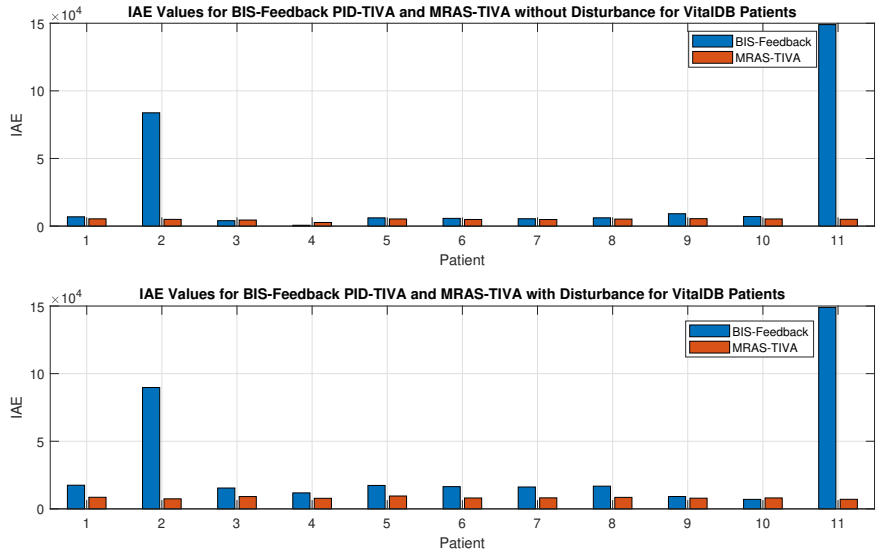

Figure 3.24 : Comparison of IAE values between BIS-Feedback PID-TIVA and MRAS-TIVA on VitalDB patients.

Similarly to previous results, the IAE values of MRAS-TIVA are lower than BIS-Feedback PID-TIVA on VitalDB patients for both cases with and without stimuli disturbances. Moreover, stability issues did not occur in MRAS-TIVA.

Overall, the proposed model reference adaptive control system structure for total intravenous anesthesia (MRAS-TIVA) has produced more robust and more desired results than one of the most common controllers, PID-TIVA, on control of total intravenous anesthesia in terms of both intra- and inter-patient validity. The systems using MRAS-TIVA can developed and operated in control of the patient's hypnotic states during total intravenous anesthesia.

4. CONCLUSIONS AND DISCUSSIONS

The main goal of the thesis was to propose a method to improve TIVA models by incorporating additional output delays using real surgical patient data. These enhanced models were expected to generate a stronger correlation between actual and simulated outputs of the same patient models. Additionally, the thesis suggested a controller structure for CL-TIVA that delivered better performance than the common PID-TIVA controllers, in intra- and inter-patient operations. The suggested controller was a model reference adaptive controller, and the adaptation laws were generated by Lyapunov's theory. This MRAC controller was expected to produce lower integral-absolute-error values than classical PID-TIVA structures, even when there was blood loss and stimuli disturbances.

The pharmacokinetic-pharmacodynamical patient models are presented with a brief introduction to compartmental modeling techniques. The Schinder PKPD parameters are explained alongside the nonlinear Hill curve equations. The effect of hemorrhage during surgeries on patient models is explained, with the stimuli disturbances that disrupt unconsciousness. The 24-patient DB is used to analyze and investigate patient models by providing patient parameters such as age, height, weight, gender, C_{50}, E_{50}, and γ. The nominal patient parameters are obtained from the mean values of parameters in 24-patient DB. The patient models are also obtained using LSE system identification from the real surgical patient database VitalDB, alongside the linear approximation of nonlinear hill curves. Moreover, delayed patient models of TIVA and a methodology for individual output delay estimation of delayed TIVA models with real surgical patient data are introduced.

Correlation analysis between real output data from VitalDB and identified model outputs has been conducted to show the correlation of results and the viability of identified models. The results of the correlation analysis have shown that the models obtained through the least squares method for the CE output have produced strong

or very strong correlation coefficients with real surgical data. However, the models obtained through the least squares method for the BIS output have not achieved the desired correlation with the actual data. It is thought that this situation may be due to measurement noise and monitor delays from the BIS monitor. Accordingly, the hypothesis has been formulated that by adding monitor delay to the linearized patient model with BIS output, higher correlation between model outputs and real data can be achieved.

The methodology for estimating the delay of delayed patient models consists of least squares error-based system identification from VitalDB data using DARX polynomial models for the parametric transfer functions of patient models. The output delay value that produces the highest correlation with real surgical data was considered the specific delay value of each patient. The validity of the delayed models was proven by comparing correlations between delayed and non-delayed model outputs and real surgical output data. The correlation analysis results indicate that patient models, which include output delays in pharmacokinetic-pharmacodynamic (PKPD) analysis, show stronger correlations with actual patient data from VitalDB. The significance is particularly notable in cases where BIS is chosen as the output variable.

Control of TIVA has also been studied in this thesis starting with explaining performance criteria and limitations of CL-TIVA. The BIS aim of CL-TIVA is 50. The performance criteria have been determined as a maximum of 5 minutes of settling time and less overshoot than %10 during the induction phase. The performance criteria of the maintenance phase is to maintain the BIS value of 50 between the values of 40-60 during the surgery. The control methods were designed according to these criteria and controller performances were evaluated using IAE. The common CL-TIVA controller PID-TIVA was presented with two different structures as CE-Feedback and BIS-Feedback. The CE-Feedback structure takes CE value as the main feedback source using additional filtering methods while BIS-Feedback takes BIS value as the main feedback source without any additional filters. These PID-TIVA structures performed acceptable results for the 24-patient database, while significant robustness issues are observed for VitalDB-identified patients.

A MRAS structure for CL-TIVA is introduced for intra- and inter-patient validity. The MRAS-TIVA structure is based on an observer-based state feedback controller. The adaptation laws generated using Lyapunov's stability theory adjust the SFC gains to ensure inter-patient validity. The MRAC was implemented for MRAS-TIVA and tested for both 24-patient DB and VitalDB-identified patients under the cases with and without stimuli disturbances and, more importantly, persistent blood loss. The control of total intravenous anesthesia was improved by the MRAS-TIVA, producing more robust and desirable results compared to the common PID-TIVA controller, with validity observed both within and between patients. The MRAS-TIVA system can be utilized to develop and manage the patient's hypnotic state during total intravenous anesthesia.

REFERENCES

[1] **Robinson, D.H. and Toledo, A.H.** (2012). Historical development of modern anesthesia, *Journal of Investigative Surgery*, *25*(3), 141–149.

[2] **Schiavo, M.** (2019). *Advanced Feedback Control Techniques for Intravenous Anesthesia*, University of Brescia.

[3] **Miller, T.E. and Gan, T.J.** (2015). Total intravenous anesthesia and anesthetic outcomes, *Journal of Cardiothoracic and Vascular Anesthesia*, *29*, S11–S15.

[4] **Short, C.E. and Bufalari, A.** (1999). Propofol anesthesia, *Veterinary clinics of North America: Small animal practice*, *29*(3), 747–778.

[5] **Grant, I. and Mackenzie, N.** (1985). Recovery following propofol ('Diprivan') anaesthesia–a review of three different anaesthetic techniques., *Postgraduate Medical Journal*, *61*, 133–137.

[6] **Shafer, S.L.** (1993). Advances in propofol pharmacokinetics and pharmacodynamics, *Journal of clinical anesthesia*, *5*(6), 14–21.

[7] **Schiavo, M.**, **Padula, F.**, **Latronico, N.**, **Merigo, L.**, **Paltenghi, M. and Visioli, A.** (2021). Performance evaluation of an optimized PID controller for propofol and remifentanil coadministration in general anesthesia, *IFAC Journal of Systems and Control*, *15*, 100121.

[8] **Ghita, M.**, **Neckebroek, M.**, **Muresan, C. and Copot, D.** (2020). Closed-loop control of anesthesia: Survey on actual trends, challenges and perspectives, *Ieee Access*, *8*, 206264–206279.

[9] **Fredman, B.**, **Zohar, E.**, **Philipov, A.**, **Olsfanger, D.**, **Shalev, M. and Jedeikin, R.** (1998). The induction, maintenance, and recovery characteristics of spinal versus general anesthesia in elderly patients, *Journal of Clinical Anesthesia*, *10*(8), 623–630.

[10] **Zikov, T.** (2002). *Monitoring the anesthetic-induced unconsciousness (hypnosis) using wavelet analysis of the electroencephalogram*, University of British Columbia.

[11] **Stanski, D.** (2000). Monitoring depth of anesthesia, *Anesthesia*, 1109–1113.

[12] **Singh, H.** (1999). Bispectral index (BIS) monitoring during propofol-induced sedation and anaesthesia, *European journal of anaesthesiology*, *16*(1), 31–36.

[13] **Bibian, S.**, **Ries, C.R.**, **Huzmezan, M. and Dumont, G.A.** (2003). Clinical anesthesia and control engineering: Terminology, concepts and issues, *2003 European Control Conference (ECC)*, IEEE, pp.2430–2440.

[14] **Schwilden, H.**, **Stoeckel, H. and Schüttler, J.** (1989). Closed-loop feedback control of propofol anaesthesia by quantitative EEG analysis in humans, *BJA: British Journal of Anaesthesia*, *62*(3), 290–296.

[15] **Schwilden, H. and Stoeckel, H.** (1987). Quantitative EEG analysis during anaesthesia with isoflurane in nitrous oxide at 1.3 and 1.5 MAC, *BJA: British Journal of Anaesthesia*, *59*(6), 738–745.

[16] **Rampil, I.**, **Sasse, F.**, **Smith, N.T.**, **Hoff, B. and Flemming, D.** (1980). Spectral edge frequency—a new correlate of anesthetic depth, *The Journal of the American Society of Anesthesiologists*, volume 53, The American Society of Anesthesiologists, pp.S12–S12.

[17] **Flaishon, R.**, **SEBEL, O. and Sigl, J.** (1995). BISPECTRAL ANALYSIS OF THE EEG FOR MONITORING THE HYPNOTIC EFFECT OF PROPOFOL AND PROPOFOL ALFENTANIL, *Anesthesiology*, volume 83, LIPPINCOTT-RAVEN PUBL 227 EAST WASHINGTON SQUARE, PHILADELPHIA, PA 19106, pp.A514–A514.

[18] **Rosow, C. and Manberg, P.J.** (2001). Bispectral index monitoring, *Anesthesiology Clinics of North America*, *19*(4), 947–966.

[19] **Glass, P.S.**, **Bloom, M.**, **Kearse, L.**, **Rosow, C.**, **Sebel, P. and Manberg, P.** (1997). Bispectral analysis measures sedation and memory effects of propofol, midazolam, isoflurane, and alfentanil in healthy volunteers, *The Journal of the American Society of Anesthesiologists*, *86*(4), 836–847.

[20] **Ferrier, D.C.**, **Kiely, J. and Luxton, R.** (2022). Propofol detection for monitoring of intravenous anaesthesia: a review, *Journal of Clinical Monitoring and Computing*, *36*(2), 315–323.

[21] **Nishio, T.**, **Suzuki, R.**, **Tsukada, Y.**, **Kanazawa, H.**, **Okano, T. and Miyabe-Nishiwaki, T.** (2009). Aqueous chromatographic system for the quantification of propofol in biological fluids using a temperature-responsive polymer modified stationary phase, *Journal of Chromatography A*, *1216*(44), 7427–7432.

[22] **Vishwanathan, K. and Stewart, J.T.** (1999). HPLC determination of a propofol and remifentanil mixture, *Journal of liquid chromatography & related technologies*, *22*(6), 923–931.

[23] **Dowrie, R.H.**, **Ebling, W.F.**, **Mandema, J.W. and Stanski, D.R.** (1996). High-performance liquid chromatographic assay of propofol in human and rat plasma and fourteen rat tissues using electrochemical detection, *Journal of Chromatography B: Biomedical Sciences and Applications*, *678*(2), 279–288.

[24] **Mistry, S. and Wenthold, P.G.** (2018). Mass spectrometric detection of the Gibbs reaction for phenol analysis, *Journal of mass spectrometry*, *53*(10), 947–953.

[25] **Hornuss, C.**, **Praun, S.**, **Villinger, J.**, **Dornauer, A.**, **Moehnle, P.**, **Dolch, M.**, **Weninger, E.**, **Chouker, A.**, **Feil, C.**, **Briegel, J.** *et al.* (2007). Real-time monitoring of propofol in expired air in humans undergoing total intravenous anesthesia, *The Journal of the American Society of Anesthesiologists*, *106*(4), 665–674.

[26] **Mendez, J.A.**, **Torres, S.**, **Reboso, J.A. and Reboso, H.** (2009). Model-based controller for anesthesia automation, *2009 IEEE International Conference on Automation Science and Engineering*, IEEE, pp.379–384.

[27] **Derighetti, M.P.** (1999). *Feedback control in anaesthesia*, volume 13, ETH Zurich.

[28] **Roberts, F.**, **Dixon, J.**, **Lewis, G.**, **Tackley, R. and Prys-Roberts, C.** (1988). Induction and maintenance of propofol anaesthesia: a manual infusion scheme, *Anaesthesia*, *43*, 14–17.

[29] **Schiavo, M.**, **Padula, F.**, **Latronico, N.**, **Paltenghi, M. and Visioli, A.** (2022). On the practical use of a PID-based control scheme for automatic control of general anesthesia, *2022 IEEE Conference on Control Technology and Applications (CCTA)*, IEEE, pp.1105–1110.

[30] **Morley, A.**, **Derrick, J.**, **Mainland, P.**, **Lee, B. and Short, T.** (2000). Closed loop control of anaesthesia: an assessment of the bispectral index as the target of control, *Anaesthesia*, *55*(10), 953–959.

[31] **Van Heusden, K.**, **Dumont, G.A.**, **Soltesz, K.**, **Petersen, C.L.**, **Umedaly, A.**, **West, N. and Ansermino, J.M.** (2013). Design and clinical evaluation of robust PID control of propofol anesthesia in children, *IEEE Transactions on Control Systems Technology*, *22*(2), 491–501.

[32] **Gonzalez-Cava, J.M.**, **Carlson, F.B.**, **Troeng, O.**, **Cervin, A.**, **van Heusden, K.**, **Dumont, G.A. and Soltesz, K.** (2021). Robust PID control of propofol anaesthesia: uncertainty limits performance, not PID structure, *Computer Methods and Programs in Biomedicine*, *198*, 105783.

[33] **Schiavo, M.**, **Padula, F.**, **Latronico, N.**, **Paltenghi, M. and Visioli, A.** (2022). A modified PID-based control scheme for depth-of-hypnosis control: Design and experimental results, *Computer Methods and Programs in Biomedicine*, *219*, 106763.

[34] **Ionescu, C.M.**, **De Keyser, R.**, **Torrico, B.C.**, **De Smet, T.**, **Struys, M.M. and Normey-Rico, J.E.** (2008). Robust predictive control strategy applied for propofol dosing using BIS as a controlled variable during anesthesia, *IEEE Transactions on biomedical engineering*, *55*(9), 2161–2170.

[35] **Hosseinzadeh, M.**, **van Heusden, K.**, **Yousefi, M.**, **Dumont, G.A. and Garone, E.** (2020). Safety enforcement in closed-loop anesthesia—A comparison study, *Control Engineering Practice*, *105*, 104653.

[36] **Soltesz, K.**, **Hahn, J.O.**, **Dumont, G.A. and Ansermino, J.M.** (2011). Individualized PID control of depth of anesthesia based on patient model identification during the induction phase of anesthesia, *2011 50th IEEE Conference on Decision and Control and European Control Conference*, IEEE, pp.855–860.

[37] **Nascu, I.**, **Nascu, I.**, **Ionescu, C.M. and De Keyser, R.** (2012). Adaptive EPSAC predictive control of the hypnotic component in anesthesia, *Proceedings of 2012 IEEE international conference on automation, quality and testing, robotics*, IEEE, pp.103–108.

[38] **Nino, J.**, **De Keyser, R.**, **Syafiie, S.**, **Ionescu, C. and Struys, M.** (2009). EPSAC-controlled anesthesia with online gain adaptation, *International journal of adaptive control and signal processing*, *23*(5), 455–471.

[39] **Glass, P.S. and Rampil, I.J.** (2001). Automated anesthesia: Fact or fantasy?, *The Journal of the American Society of Anesthesiologists*, *95*(1), 1–2.

[40] **Absalom, A.R.**, **De Keyser, R. and Struys, M.M.** (2011). Closed loop anesthesia: are we getting close to finding the holy grail?, *Anesthesia & Analgesia*, *112*(3), 516–518.

[41] **Haddad, W.M.**, **Hayakawa, T. and Bailey, J.M.** (2003). Nonlinear adaptive control for intensive care unit sedation and operating room hypnosis, *Proceedings of the 2003 American Control Conference, 2003.*, volume 2, IEEE, pp.1808–1813.

[42] **Northrop, R.B.** (2020). *Endogenous and exogenous regulation and control of physiological systems*, CRC Press.

[43] **Enderle, J. and Bronzino, J.** (2012). *Introduction to biomedical engineering*, Academic press.

[44] **Van Milligen, B.P.**, **Bons, P.**, **Carreras, B.A. and Sanchez, R.** (2005). On the applicability of Fick's law to diffusion in inhomogeneous systems, *European journal of physics*, *26*(5), 913.

[45] **Godfrey, K.** (1983). Compartmental models and their application, *Academic Press, London*.

[46] **Naşcu, I.**, **Krieger, A.**, **Ionescu, C.M. and Pistikopoulos, E.N.** (2014). Advanced model-based control studies for the induction and maintenance of intravenous anaesthesia, *IEEE Transactions on biomedical engineering*, *62*(3), 832–841.

[47] **Schiavo, M.** (2022). *Automatic Control of General Anesthesia: New Developments and Clinical Experiments*, University of Brescia.

[48] **Nunes, C.S.**, **Mendonça, T.**, **Lemos, J.M. and Amorim, P.** (2009). Feedforward adaptive control of the Bispectral Index of the EEG using the intravenous anaesthetic drug propofol, *International journal of adaptive control and signal processing*, *23*(5), 485–503.

[49] **Minto, C. and Schnider, T.** (2008). Contributions of PK/PD modeling to intravenous anesthesia, *Clinical pharmacology & therapeutics*, *84*(1), 27–38.

[50] **Schnider, T.W.**, **Minto, C.F.**, **Gambus, P.L.**, **Andresen, C.**, **Goodale, D.B.**, **Shafer, S.L. and Youngs, E.J.** (1998). The influence of method of administration and covariates on the pharmacokinetics of propofol in adult volunteers, *The Journal of the American Society of Anesthesiologists*, *88*(5), 1170–1182.

[51] **Ionescu, C.M.**, **De Keyser, R.**, **Torrico, B.C.**, **De Smet, T.**, **Struys, M.M. and Normey-Rico, J.E.** (2008). Robust predictive control strategy applied for propofol dosing using BIS as a controlled variable during anesthesia, *IEEE Transactions on biomedical engineering*, *55*(9), 2161–2170.

[52] **Ionescu, C.M.**, **Neckebroek, M.**, **Ghita, M. and Copot, D.** (2021). An open source patient simulator for design and evaluation of computer based multiple drug dosing control for anesthetic and hemodynamic variables, *IEEE Access*, *9*, 8680–8694.

[53] **Johansen, J.W.** (2006). Update on bispectral index monitoring, *Best practice & research Clinical anaesthesiology*, *20*(1), 81–99.

[54] **Ionescu, C.M.** (2018). A computationally efficient Hill curve adaptation strategy during continuous monitoring of dose–effect relation in anaesthesia, *Nonlinear Dynamics*, *92*(3), 843–852.

[55] **Hemmings, H.C. and Egan, T.D.** (2012). *Pharmacology and physiology for anesthesia e-book: foundations and clinical application*, Elsevier Health Sciences.

[56] **Ghita, M.**, **Copot, D.**, **Birs, I.**, **Muresan, C.**, **Neckebroek, M. and Ionescu, C.** (2023). Modelling of Blood Loss Influence on Propofol Concentrations and Anesthetic States in Critical Responses, *2023 American Control Conference (ACC)*, IEEE, pp.2216–2221.

[57] **West, N.**, **Dumont, G.A.**, **Van Heusden, K.**, **Petersen, C.L.**, **Khosravi, S.**, **Soltesz, K.**, **Umedaly, A.**, **Reimer, E. and Ansermino, J.M.** (2013). Robust closed-loop control of induction and maintenance of propofol anesthesia in children, *Pediatric Anesthesia*, *23*(8), 712–719.

[58] **Ionescu, C.M.**, **Nascu, I. and De Keyser, R.** (2011). Robustness tests of a model based predictive control strategy for depth of anesthesia regulation in a propofol to bispectral index framework, *International Conference on Advancements of Medicine and Health Care through Technology:*

29th August–2nd September 2011, Cluj-Napoca, Romania, Springer, pp.234–239.

[59] **Yelneedi, S.**, **Samavedham, L. and Rangaiah, G.** (2009). Advanced control strategies for the regulation of hypnosis with propofol, *Industrial & engineering chemistry research*, *48*(8), 3880–3897.

[60] **Jeong, J.H.**, **Lee, B.**, **Hong, J.**, **Min, C.**, **Persad, A.R.**, **Yang, T.H. and Park, Y.H.** (2024). Cardiovascular hardware simulator and artificial aorta-generated central blood pressure waveform database according to various vascular ages for cardiovascular health monitoring applications, *Computers in Biology and Medicine*, *172*, 108224.

[61] **Chen, M.**, **He, Y. and Yang, Z.** (2023). A Deep Learning Framework for Anesthesia Depth Prediction from Drug Infusion History, *Sensors*, *23*(21), 8994.

[62] **Lee, H.C.**, **Park, Y.**, **Yoon, S.B.**, **Yang, S.M.**, **Park, D. and Jung, C.W.** (2022). VitalDB, a high-fidelity multi-parameter vital signs database in surgical patients, *Scientific Data*, *9*(1), 279.

[63] **Moussa, K.**, **Aubouin-Pairault, B.**, **Alamir, M. and Dang, T.** (2023). Data-based Extended Moving Horizon Estimation for MISO Anesthesia Dynamics, *IEEE Control Systems Letters*.

[64] **Senthilnathan, S.** (2019). Usefulness of correlation analysis, *Available at SSRN 3416918*.

[65] **Gogtay, N.J. and Thatte, U.M.** (2017). Principles of correlation analysis, *Journal of the Association of Physicians of India*, *65*(3), 78–81.

[66] **Ratner, B.** (2009). The correlation coefficient: Its values range between+ 1/- 1, or do they?, *Journal of targeting, measurement and analysis for marketing*, *17*(2), 139–142.

[67] **MacDonald, N. and Lags, T.** (1978). Lecture notes in biomathematics, *Springer*, *17*, 1059–1062.

[68] **Hu, S.**, **Dunlavey, M.**, **Guzy, S. and Teuscher, N.** (2018). A distributed delay approach for modeling delayed outcomes in pharmacokinetics and pharmacodynamics studies, *Journal of Pharmacokinetics and Pharmacodynamics*, *45*, 285–308.

[69] **Ferreira, A.L.**, **Mendes, J.G.**, **Nunes, C.S. and Amorim, P.** (2019). Evaluation of Bispectral Index time delay in response to anesthesia induction: an observational study, *Revista brasileira de anestesiologia*, *69*, 377–382.

[70] **Söderström, T. and Stoica, P.** (1988). *System identification*, Prentice-Hall, Inc., USA.

[71] **Pawłowski, A.**, **Schiavo, M.**, **Latronico, N.**, **Paltenghi, M. and Visioli, A.** (2022). Model predictive control using MISO approach for drug co-administration in anesthesia, *Journal of Process Control*, *117*, 98–111.

[72] **Nguyen, N.T.** (2018). Model-Reference Adaptive Control, Springer International Publishing, Cham, pp.83–123, https://doi.org/10.1007/978-3-319-56393-0_5.

[73] **Soderstrom, T. and Stoica, P.** (1989). *System Identification*, Prentice-Hall International, Hemel Hempstead, U.K.

[74] **Simon, D.** (2006). *Optimal state estimation: Kalman, H infinity, and nonlinear approaches*, John Wiley & Sons.

[75] **Aubouin-Pairault, B.**, **Fiacchini, M. and Dang, T.** (2024). Comparison of multiple Kalman filter and moving horizon estimator for the anesthesia process, *Journal of Process Control*, *136*, 103179.

[76] **Astrom, K.J. and Wittenmark, B.** Adaptive control, 1995, *Addision-Wesley Publishing Company*.

[77] **Brogliato, B.**, **Lozano, R.**, **Maschke, B.**, **Egeland, O.**, **Brogliato, B.**, **Lozano, R.**, **Maschke, B. and Egeland, O.** (2020). Kalman–Yakubovich–Popov Lemma, *Dissipative Systems Analysis and Control: Theory and Applications*, 81–261.

APPENDICES

APPENDIX A : Patient Databases
APPENDIX B : PID-TIVA IAE Values
APPENDIX C : MRAS-TIVA IAE Values

APPENDIX A : Patient Databases

Table A.1 : Patient database for 24 people

Index	**Age**	**Height**	**Weight**	C_{50}	γ
1	74	164	88	2.5	3
2	67	161	69	4.6	2
3	75	176	101	5	1.6
4	69	173	97	1.8	2.5
5	45	171	64	6.8	1.78
6	57	182	80	2.7	2.8
7	74	155	55	1.7	3.5
8	71	172	78	7.8	2.9
9	65	176	77	2.9	1.88
10	72	192	73	3.9	3.1
11	69	168	84	2.3	3.1
12	60	190	92	4.8	2.1
13	61	177	81	2.5	3
14	54	173	86	2.5	3
15	71	172	83	4.3	1.9
16	53	186	114	2.7	1.6
17	72	162	87	4.5	2.9
18	61	182	93	2.7	1.78
19	70	167	77	6.8	3.1
20	69	168	82	9.8	1.6
21	69	158	81	3.2	2.1
22	60	165	85	5.1	2.51
23	70	173	69	3.67	3.1
24	56	186	99	5.8	2.3

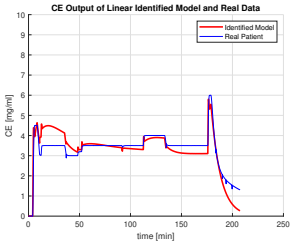

((a)) Patient 1

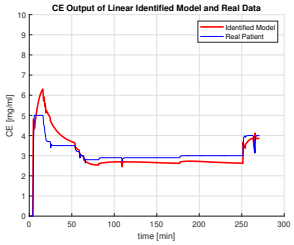

((b)) Patient 2

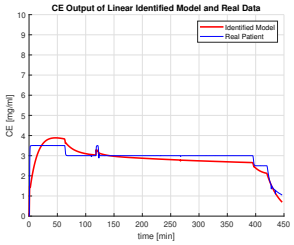

((c)) Patient 3

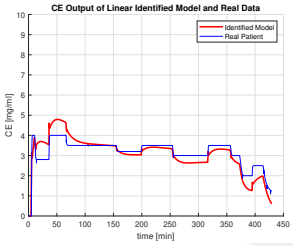

((d)) Patient 4

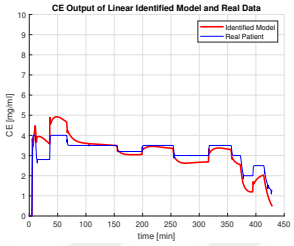

((e)) Patient 5

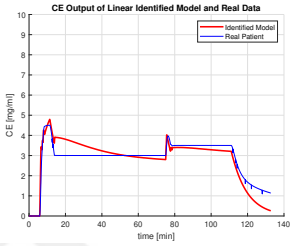

((f)) Patient 6

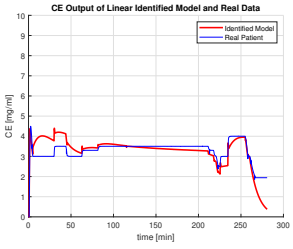

((g)) Patient 7

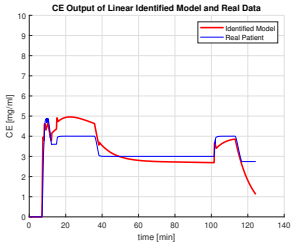

((h)) Patient 8

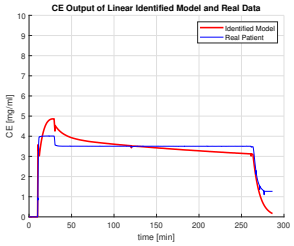

((i)) Patient 9

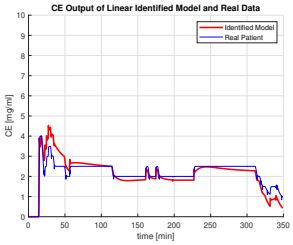

((j)) Patient 10

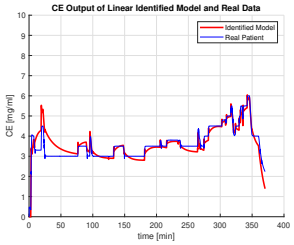

((k)) Patient 11

Figure A.1 : CE Output of Linear Identified Model and Real Data for 11 patients from VitalDB

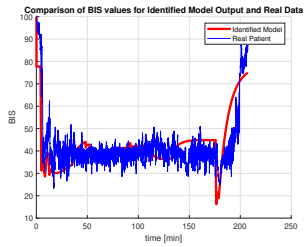

((a)) Patient 1

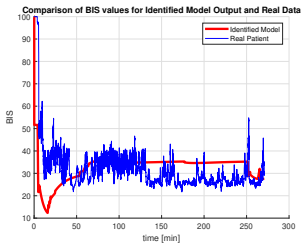

((b)) Patient 2

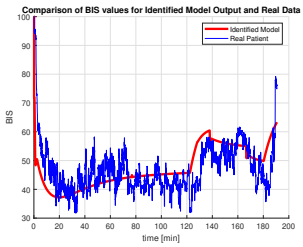

((c)) Patient 3

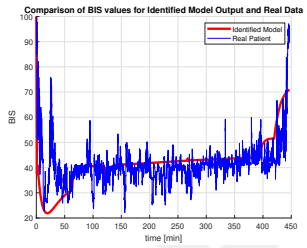

((d)) Patient 4

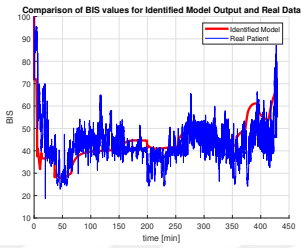

((e)) Patient 5

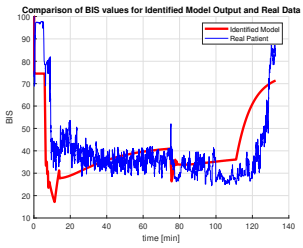

((f)) Patient 6

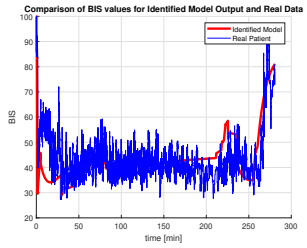

((g)) Patient 7

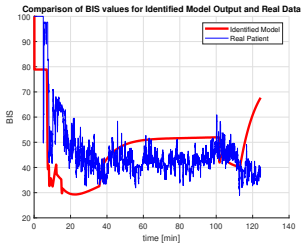

((h)) Patient 8

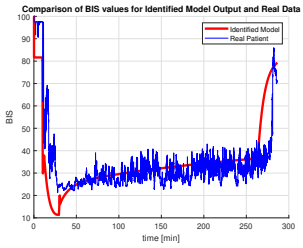

((i)) Patient 9

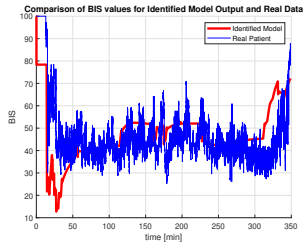

((j)) Patient 10

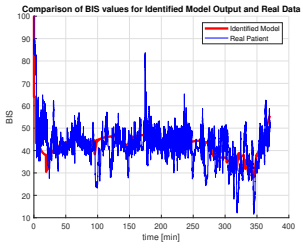

((k)) Patient 11

Figure A.2 : Comparison of BIS values for identified model output and real data for 11 patients from VitalDB

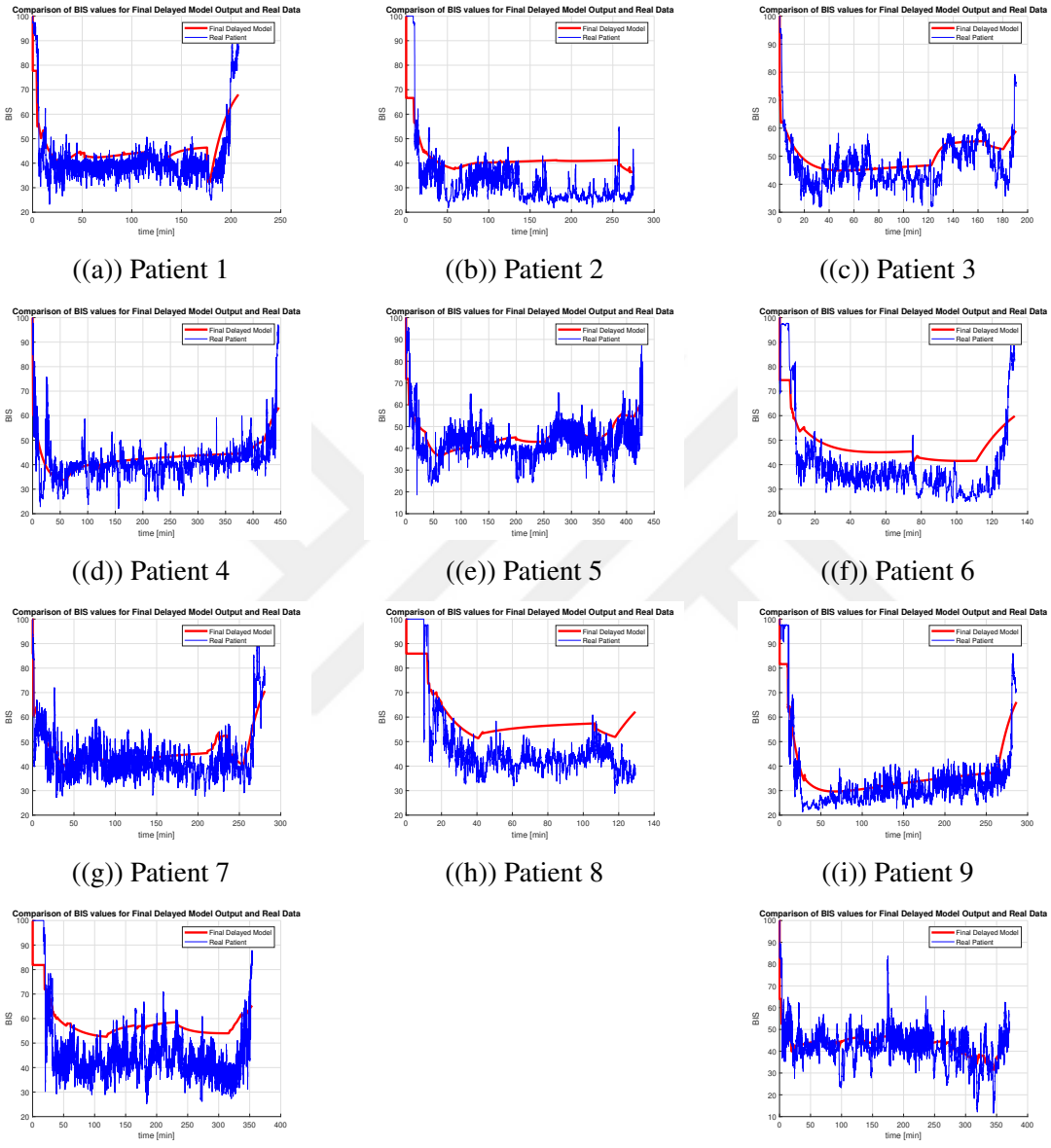

((a)) Patient 1 ((b)) Patient 2 ((c)) Patient 3

((d)) Patient 4 ((e)) Patient 5 ((f)) Patient 6

((g)) Patient 7 ((h)) Patient 8 ((i)) Patient 9

((j)) Patient 10 ((k)) Patient 11

Figure A.3 : Comparison of BIS values for final delayed model output and real data for 11 patients from VitalDB

APPENDIX B : PID-TIVA IAE Values

Table B.1 : IAE values of PID-TIVA

Patient	Non-Disturbance		Disturbance	
	CE-Feedback	**BIS-Feedback**	**CE-Feedback**	**BIS-Feedback**
Patient 1	5345	7867	12951	15905
Patient 2	7315	10890	15943	19568
Patient 3	7982	12160	16984	20830
Patient 4	4648	6449	12146	14474
Patient 5	9763	14816	18766	23759
Patient 6	5724	8495	13434	16652
Patient 7	4204	5999	11484	13981
Patient 8	10411	16890	18805	24565
Patient 9	5799	8242	14062	16981
Patient 10	6858	10614	14722	18784
Patient 11	5125	7501	12637	15492
Patient 12	8034	12415	16574	20745
Patient 13	5434	8031	13032	16060
Patient 14	5539	8232	13100	16241
Patient 15	7136	10622	15765	19293
Patient 16	6045	8745	14517	17547
Patient 17	7489	11706	15496	19886
Patient 18	5742	8160	13984	16897
Patient 19	9543	15408	17795	23257
Patient 20	11772	18159	20888	26999
Patient 21	6087	8842	14294	17461
Patient 22	8246	12931	16569	21085
Patient 23	6527	9978	14438	18209
Patient 24	9320	14806	17812	22771
Mean	**7408**	**11364**	**15834**	**19696**

APPENDIX C : MRAS-TIVA IAE Values

Table C.1 : IAE values of MRAS-TIVA

Patient	**Non-disturbance**	**Disturbance**
Patient 1	6502	13361
Patient 2	8188	15562
Patient 3	8533	16214
Patient 4	5742	12650
Patient 5	9953	17811
Patient 6	6827	13694
Patient 7	5276	12904
Patient 8	10890	17881
Patient 9	6750	14069
Patient 10	7986	14812
Patient 11	6274	13074
Patient 12	8716	15824
Patient 13	6572	13394
Patient 14	6663	13341
Patient 15	7988	15291
Patient 16	6866	13923
Patient 17	8505	15357
Patient 18	6665	13828
Patient 19	10264	17151
Patient 20	11369	19570
Patient 21	7083	14339
Patient 22	9014	15907
Patient 23	7697	14713
Patient 24	9713	16781
Mean	**7918.17**	**14824.79**

CURRICULUM VITAE

Name SURNAME: Bora Ayvaz

EDUCATION:

- **B.Sc.:** 2022, Istanbul Technical University, Faculty of Electrical and Electronics Engineering, Control and Automation Engineering Department
- **M.Sc.:** 2024 (Expected), Istanbul Technical University, Graduation School, Control and Automation Engineering Program

PROFESSIONAL EXPERIENCE AND REWARDS:

- 2022-Present, Istanbul Technical University, Research Assistant.

PUBLICATIONS, PRESENTATIONS AND PATENTS ON THE THESIS:
OTHER PUBLICATIONS, PRESENTATIONS AND PATENTS:

- **Ayvaz, B.** , İlikçi, H., Bilgili, F., Ergenç, A. F. (2023, October). IoT Networks and Online Image Processing in IMU-Based Gait Analysis. In International Conference on IoT and Health (pp. 162-177). Cham: Springer Nature Switzerland.
- Yapakçı, B., Akdağcık, Z., **Ayvaz, B.**, Ergenç, A. F. (2023, October). Application of Process Mining to Production Lines Using Industrial Internet of Things. In 2023 IEEE 5th Eurasia Conference on IOT, Communication and Engineering (ECICE) (pp. 347-352). IEEE.